

# **STUDY OF RAMAN ANTENNA EFFECTS OF ANISOTROPIC PLASMONIC METAL NANOSTRUCTURES**

A thesis submitted to  
Indian Institute of Science Education and research  
towards partial fulfilment of  
BS-MS Dual Degree Programme

by

**HARSHVARDHAN JOG**

REG. No. 20121100

under the guidance of

DR. G.V. PAVAN KUMAR



INDIAN INSTITUTE OF SCIENCE EDUCATION AND RESEARCH PUNE

DR. HOMI BHABHA ROAD  
PASHAN, PUNE 411008, INDIA

April 2017

©Harshvardhan Jog 2017

All rights reserved



# Certificate

This is to certify that this thesis entitled "Study of Raman Antenna Effects of Anisotropic Plasmonic Metal Nanostructures" submitted towards the partial fulfilment of the BS-MS dual degree programme at the Indian Institute of Science Education and Research Pune represents original research carried out by HARSHVARDHAN JOG at the Indian Institute of Science Education and Research, Pune, under the supervision of DR. G.V.PAVAN KUMAR during the academic year 2016-2017.



Student

HARSHVARDHAN JOG



Supervisor


DR. G.V.PAVAN KUMAR





# Declaration

I hereby declare that the matter embodied in the report entitled "Study of Raman Antenna Effects of Anisotropic Plasmonic Metal Nanostructures" are the results of the investigations carried out by me at the Department of Physics, Indian Institute of Science Education and Research Pune, under the supervision of Dr. G.V. Pavan Kumar and the same has not been submitted elsewhere for any other degree.



Student

HARSHVARDHAN JOG



Supervisor

DR. G.V. PAVAN KUMAR



# Acknowledgements

This thesis, and all the research I have done in the past year alongside it has been with the help of several people whom I would like to thank here.

Firstly, I would like to thank Dr. G.V.Pavan Kumar, who has been my guide for the past two years, and has given me his valuable advice and directions as to where I should proceed. He has always supported me when I did something correctly, and corrected me whenever it was required. Discussions with him have always given me new insights, be it about research, or about selection of my future path towards Doctoral research. I am really thankful to have had a guide who gave freedom in terms of many things, as long as the required work was done properly.

I would like to thank Adarsh Vasista, who is currently pursuing his doctoral research in Dr. Pavan Kumar's lab. He has been a mentor, whose knowledge about optics and plasmonics has helped me countless number of times. Working with him has been fun (not without arguments and disagreements of course, but fun nonetheless!), and it has made this project into something of real academic value.

I would like to thank Danveer Singh, who synthesized the wires that were used for the project. I would also want to thank Ravi Tripathi for giving his after-hours time for SEM imaging of the structures I synthesized in the lab. I would like to thank Dr. Debrina Jana and Dr. Parthapratim Patra for helping me with technical details about synthesis procedures and other related things.

My time in the lab was made really interesting by my labmates: Rajath Sawant, Deepak Kumar Sharma, Ravi Tripathi, Vandana Sharma, Shailendra Chaubey, Sunny Tiwari, and Jesil Jose, who made the daily chai time into a discussion forum for everything from research to politics to IISER gossip. Of course, I would also like mention the MDP guys, who fuelled the my day with chai in the afternoon as well as late at night. Special mention goes to all my friends, who have made this journey enjoyable through all the lunch and dinner table conversations, as well as the random hangout sessions and parties.

Finally, I want to express my deep gratitude towards my father and mother, who have always supported me and believed in me, whatever choices I make in life. Their constant concern for me has helped me be focused and given me inspiration to work towards my chosen goal.

Truly,

Harshvardhan Jog



# Abstract

The interactions of 0D and 1D nanostructures with a 2D plasmonic film have seldom been studied in literature. The cavity or the "hot-spot" that forms between the nanostructure and the film are interesting structures, as the field is highly confined and enhanced in these regions. Thus, placing Raman active dyes in these locations will lead to huge enhancement of the Raman signal obtained from them. The structures will also have antenna effects, which will lead to the radiation properties, such as directionality and polarization states, being changed according to the geometry of the structures. As the Raman antenna effects of such structures have not been probed in great detail in literature, this project aims to do so for two anisotropic nanostructures, gold nanorods and silver nanowires.

The first chapter gives an introduction about the concepts that are necessary to understand the effects observed in the thesis. This includes an introduction to plasmons and various related concepts, antenna effects, and molecular emission processes.

The second chapter mainly deals with the synthesis of symmetric and asymmetric metal nanoparticles, which includes Au nanospheres, Au nanotriangles and Au nanorods. Such structures are important for the experimental studies that have been done later in the thesis.

The third chapter details the experimental studies done on Au nanorods and Ag nanowires placed over gold films, which act as plasmonic mirrors. The studies consist of observation of enhancement, input polarization dependence of the SERS signal, and in case of Ag nanowires, remote excitation experiments wherein one end of the wire is excited and the signal is collected and analyzed at the distal end.

The fourth chapter investigates the simulation aspects of the Ag nanowire-over-gold film system. Simulations were done to corroborate the experimental results obtained in chapter 3. Simulations have also been done to gain insights about the system that can not be obtained experimentally. Thus simulations have been used both as a tool to aid experiments as well as to guide experiments in further directions.



# Contents

<b>1</b>	<b>Introduction</b>	<b>7</b>
1.1	Plasmonics: A primer . . . . .	8
1.1.1	Localized Surface Plasmons . . . . .	10
1.1.2	Surface Plasmon Polaritons . . . . .	11
1.1.3	Gap and cavity plasmons . . . . .	13
1.2	Antenna parameters . . . . .	13
1.3	Molecular Emissions and Scattering processes . . . . .	15
1.3.1	Fluorescence . . . . .	16
1.3.2	Raman scattering . . . . .	17
1.4	Definition and Motivation of Thesis problem . . . . .	19
<b>2</b>	<b>Synthesis of Symmetric and Asymmetric Gold Nanoparticles</b>	<b>21</b>
2.1	Synthesis of Gold nanospheres . . . . .	22
2.2	Synthesis of Gold nanotriangles . . . . .	22
2.3	Synthesis of Gold nanorods . . . . .	24
<b>3</b>	<b>Study of Antenna Effects of Asymmetric Metal Nanoparticles</b>	<b>26</b>
3.1	Optical studies of Au nanorods on Gold film . . . . .	27
3.1.1	Experimental setup and basic results . . . . .	28
3.1.2	Polarization dependence of SERS signal . . . . .	30
3.1.3	Limitations . . . . .	31
3.2	Optical studies of Ag nanowires on gold film . . . . .	31
3.2.1	Enhancement and Polarization dependence of SERS signals . . . . .	34
3.2.2	Remote excitation SERS . . . . .	36
3.2.3	Conclusions for Chapter 3 . . . . .	47
<b>4</b>	<b>Simulation studies of Ag wire on Au film system</b>	<b>48</b>
4.1	Basic parameter details . . . . .	49
4.2	Input polarization dependence for center excitation . . . . .	50
4.2.1	Leakage Radiation of chiral plasmons . . . . .	52
4.3	End fire configuration . . . . .	53

4.3.1	Polarization: Input angle dependence . . . . .	54
4.3.2	Polarization: Output angle dependence . . . . .	56
<b>5</b>	<b>Conclusions and Future Outlook</b>	<b>59</b>
	<b>References</b>	<b>61</b>



# List of Figures

1.1	Surface plasmon characteristics . . . . .	9
1.2	Schematic for theory; SP dispersion diagram . . . . .	11
1.3	Antenna structure . . . . .	14
1.4	Energy level diagram of fluorescent molecule . . . . .	15
1.5	Various scattering phenomena in molecules . . . . .	17
2.1	SEM images and UV-Vis spectra of various nanoparticles that were synthesized	23
3.1	Nile Blue molecular structure . . . . .	27
3.2	Schematic of Au rod on Au film system . . . . .	28
3.3	Schematic of setup used for enhancement and polarization dependent measurements . . . . .	29
3.4	Raman spectra observed from various particles; Polarization dependence of SERS spectra . . . . .	30
3.5	Optical and SEM image of single Ag nanowire on Au film . . . . .	32
3.6	Fluorescence spectrum observed for Ag wire on glass . . . . .	33
3.7	Schematic of Ag wire on Au film system used for polarization dependence experiments . . . . .	33
3.8	Enhancement of NB Raman spectrum due to Ag wire-on-Au film system; Polarization dependence of the $590\text{cm}^{-1}$ line; Simulation results . . . . .	35
3.9	Schematic of setup used for remote excitation experiments . . . . .	37
3.10	Schematic of Ag NW on Au film system in remote excitation geometry . . . . .	38
3.11	Optical image showing remote excitation; Remote excitation spectra of NB on glass and Au film . . . . .	39
3.12	Spectra showing signal at center of the wire vs signal at the distal end . . . . .	40
3.13	Input polarization dependence of spectra at distal end . . . . .	41
3.14	Output polarization dependence: Comparative graph for two orthogonal polarizations . . . . .	43
3.15	Output polarization dependence: Oscillations in longitudinal polarization . . . . .	43
3.16	Input power dependence at the excitation end and distal end . . . . .	45
3.17	Effect of spacer layer placed on Au film . . . . .	46

4.1	Parameters used for simulations . . . . .	49
4.2	Charge distribution for various input polarizations with excitation at center . . .	51
4.3	Leakage radiation towards glass side for thin film . . . . .	53
4.4	Remote excitation: Generation of SPP and Gap plasmon . . . . .	54
4.5	Remote excitation: Input polarization dependence . . . . .	55
4.6	Cross sectional field profile for two orthogonal input polarizations . . . . .	56
4.7	Field profiles in the gap for $E_x$ and $E_y$ . . . . .	57
4.8	Field profiles for 3 edges for the components $E_x$ and $E_y$ . . . . .	58

# Chapter 1

## Introduction

Antennas have been in use in human lives for over a century now. The first antenna was built by physicist Heinrich Hertz to demonstrate Maxwell's theory on electromagnetism [1], which was later perfected by the Italian inventor and Nobel laureate Guglielmo Marconi. Marconi successfully harnessed the power of antenna effects in the radio frequencies in 1895 to built the first radio.[2] This later revolutionized human lives, as can be seen from the ubiquity and indispensability of wireless devices ranging from WLAN, television antennas to mobile phones. The technology has been successfully modified for radio and microwave frequencies and integrated with electronics to provide high specificity, high fidelity and ultra-fast speeds in communication between the transmitters and the receivers. Antennas, therefore, have been used to successfully control electromagnetic radiation in the radio and microwave frequencies for a long time.[3]

Despite the success of antennas in the higher wavelength regimes of the electromagnetic radiation, it has been difficult to emulate the same in optical frequencies, mainly because of the wavelengths in consideration being only few hundreds of nanometers. For antennas to work in particular frequency ranges, the dimensions of the antenna have to be of the order of the wavelength in consideration.[4] Historically, before the advent of nano-science, manipulation and structuring of matter at a nano-level was a difficult task. After several decades of research into synthesis procedures for nano-materials, inventions of sophisticated instrumentation such as scanning electron microscopy (SEM) and electron-beam lithography (EBL) and other fabrication methods, it has now become possible to design structures with accuracies down to tens of nanometers. Optical antenna effects have now been successfully demonstrated by fabricating samples using electron-beam lithography [5, 6, 7], nanosphere lithography [8, 9], and with particles synthesized using wet-synthesis methods [10, 11]. It is thus possible now to fabricate optical antennas with desired properties and apply them for uses such as spectroscopy [10], optoelectronics [12], photosensors [13], directional emitters [5], to name a few.

It is a necessity that the antenna structure efficiently converts propagating electromagnetic radiation from the far-field to enhanced and localized fields in the near-field. Plasmonic nanostructures provide large field enhancements at sharp features, field confinement in gap structures, impedance matching to propagating waves to be converted from far-field ra-

diation to near-field radiation, and can be tuned in size such that the resonance of the plasmon modes lies in the region of interest.[14] Thus, plasmonic nanostructures have been a major candidate for optical antennas, and a large body of research is present to that effect. [5, 6, 7, 9, 10, 11, 13, 14, 15, 16, 17, 18, 19, 20, 21, 22] Much of this research has been towards development of antennas with high enhancement factor and high directivity. However, not much work has been done in terms of using these structures as Raman antennas, and major challenges remain in terms of optimizing the antennas in terms of highly unidirectional and enhanced emission, and impedance matching between source and antenna structure, among other things.[4] The following sections detail the necessary theoretical background for plasmonic nano-antennas, followed by a primer on molecular emission, followed by the definition and motivation for the problem addressed in this thesis.

## 1.1 Plasmonics: A primer

Ultra-fast communications have become extremely important in recent era, where everything is digitized and connected. Semiconductor-based technology has been relying on miniaturization of circuitry to cater to the ever-increasing demands of the world, in terms of performance, high density data packaging, and speed.[23] These systems have been extensively optimized and miniaturized to the point that on-chip electronic circuit elements are now reaching dimensions as small as tens of nanometers.[24] However, the fundamental limitations of these systems are now being reached, and as such, pushing the speed, performance, or information density in these systems is becoming extremely difficult. An alternative to this that is now being explored extensively is to use light instead of electrons as the information carrier. However, one of the major problems in using light for such applications is the absence of required miniaturization of circuit elements and integration on chip. One of the primary reasons for this is the diffraction limit of light, which means that it is not possible to focus a beam of light such that the beam waist is lesser than half the wavelength of light (in the particular medium).[3, 23] Thus, a fundamentally different approach has to be taken to effectively communicate in nano-regimes. Plasmonics seeks to solve this issue of diffraction limit in the optical region of the electromagnetic spectrum, and can be used to efficiently focus light tightly into sub-wavelength dimensions.

The term "Plasmonics" derives from the fact that this field deals with controlling surface plasmons at metal-dielectric interfaces, and thereby using surface plasmons as the carriers of information. Surface plasmons are the collective oscillations of the electrons at the metal-dielectric interface, which can be generated by coupling visible light photons with the electrons. [3, 24, 23] Figure 1.1 shows the characteristics of a surface plasmon on a metal-dielectric interface. The properties of these surface plasmons depends on the surface structure of the metal, the excitation beam, and the dielectric environment of the metal. All of this can be effectively tuned to suit the particular need at hand[25], which makes plasmonics a powerful

substitute for on-chip electronics.

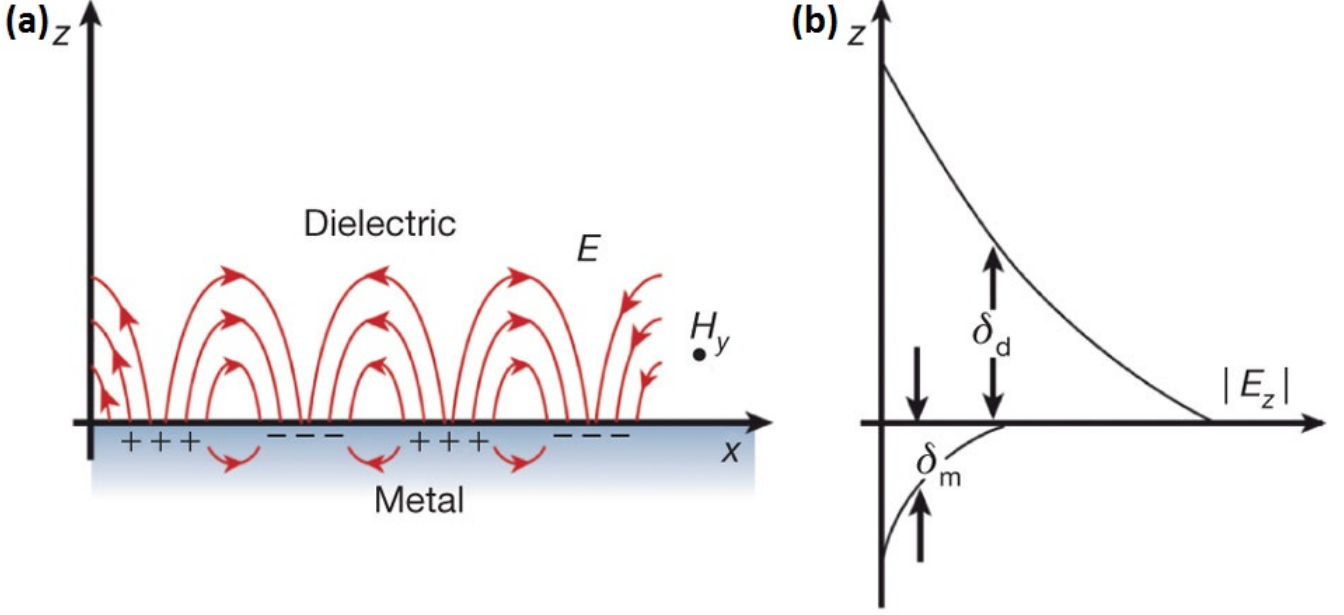


Figure 1.1: Surface plasmons on a metal dielectric interface. (a) These are transverse magnetic (TM) in nature. Surface charges are present due to a normal component of electric field at the surface ( $E_z$ ). (b)  $E_z$  component is highly enhanced near the surface, and decays exponentially along the  $z$  axis away from the surface. The decay length in the metal  $\delta_m$  is determined by the skin depth of the metal. The field in the  $z$  direction is evanescent, therefore no radiation loss occurs along this direction for SPs. Figure adapted from Ref.[25].

To give some theoretical backing to the phenomena related to plasmonics, we should first recall that for a metal, the frequency dependent dielectric function is given by the formula: [26]

$$\varepsilon(\omega) = 1 + \chi_e(\omega) \quad (1.1)$$

where  $\chi_e(\omega)$  is the electric susceptibility of the medium. To first study the effects of free electrons in the metal, we use the Drude-Sommerfeld model of free electron gas:

$$m_e \frac{\partial^2 \mathbf{r}}{\partial t^2} + m_e \Gamma \frac{\partial \mathbf{r}}{\partial t} = e E_0 e^{-i\omega t} \quad (1.2)$$

where  $m_e$  and  $e$  are the electronic mass and charge respectively,  $\mathbf{r}$  is the displacement of the electron,  $E_0$  is the amplitude of the driving electric field,  $\omega$  is the frequency of the driving field, and  $\Gamma = v_F/l$  is the damping constant, with  $v_F$  being the Fermi velocity and  $l$  being the mean free path for the electron. Solving this equation by putting  $\mathbf{r}(t) = \mathbf{r}_0 e^{-i\omega t}$  and then plugging in equation 1.1, we get:

$$\varepsilon_{Drude}(\omega) = 1 - \frac{\omega_p^2}{\omega^2 + \Gamma^2} + i \frac{\Gamma \omega_p^2}{\omega(\omega^2 + \Gamma^2)}. \quad (1.3)$$

Using experimental values for  $\omega_p$  and  $\Gamma$ , we find that the real part of  $\epsilon_{Drude}$  is negative. [26] Now, the imaginary part of the refractive index in a medium is given by  $n = \sqrt{\epsilon}$ , which implies that for metals, this has a large value. This leads to the conclusion that the field can only penetrate a metal to a very small length (called the skin depth) due to high non-radiative losses. This has been indicated in Figure 1.1.

Note that this behavior is shown by metals only in certain parts of the visible spectrum. For example, gold has a strong interband transition around 500 nm wavelength, where it absorbs large amount of the excitation light. This behavior can be derived by considering bound electrons and modifying equation 1.2 suitably to get  $\epsilon_{interband}(\omega)$ . This has been shown in greater detail in Ref[26], and will not be delved into further here.

Depending on the boundary conditions of the wave equation for electrons in metal nanoparticles coupled to the electromagnetic field, the final excitation can result in either a localized surface plasmon (LSP) or a propagating plasmon, otherwise known as surface plasmon polariton (SPP). Both these phenomena are important for different purposes, depending on the desired effects to be studied. The following subsections will give some basics about the two different phenomena.

### 1.1.1 Localized Surface Plasmons

Localized surface plasmons, as the name suggests, arise from interactions of metal nanoparticles with an oscillating electric field which leads to non-propagating excitations in the conduction electrons of the particles. Unlike the free electron case as considered while writing equation 1.2, the curvature of the surface of the metal nanoparticles exerts a restoring force on the electrons, which results in resonances. These resonances, called as localized surface plasmon resonances or LSPRs, lead to huge electric field enhancements in the near-field of the particles,[27] and are seen as peaks in the scattering spectrum. In fact, studying LSPRs is relatively easy, as they can be directly observed by examining the far-field spectra of the particles, even down to single nanoparticle limit, using white light illumination.[27, 28] The far-field spectra can be extinction spectra, which would require an ensemble or arrangement of particles, or dark-field spectra, with which one can study the LSPRs of single nanoparticles. In dark-field microscopy, one typically shines white light onto particles under study from an angle such that only the light scattered by the nanoparticles will enter the objective lens. This can be done using special dark-field apertures [28, 29], waveguide scattering microscopy [30], large angle incidence [31] or total internal reflection based imaging [32, 33, 34, 35, 36]. The spectrum, corrected for the lamp response and the dark background, gives us the dark-field spectrum of the particle under consideration, which shows the LSPRs as peaks in the spectrum. When coupled to polarization dependent studies, this technique can also give us information about various LSPR modes in anisotropic nanoparticles, which cannot otherwise be probed.[28] Another technique to probe the LSPRs is near-field optical microscopy, wherein a thin fiber tip

(with an aperture of about 100 nm) is brought in close proximity of the metal nanoparticle under study. The particle is then either excited through the tip and the response is collected in the far-field, or the particle is excited using evanescent excitation and the response is collected using the tip.[27] This also gives us the information about LSPRs in the particle under consideration.

The huge field enhancements due to LSPR and their polarization dependent response can be effectively put to use when doing Surface Enhanced Fluorescence (SEF) spectroscopy [37, 38] or Surface Enhanced Raman spectroscopy (SERS)[39, 40]. The enhancement of the electric field leads to enhancement of the molecular emission in the vicinity of the particles, and in case of anisotropic nanoparticles, this results in polarization dependent response of the molecular emission as well.[41] These effects will be discussed in terms of some theory in the section on Molecular Emissions in this chapter, and studied experimentally in Chapter 3.

### 1.1.2 Surface Plasmon Polaritons

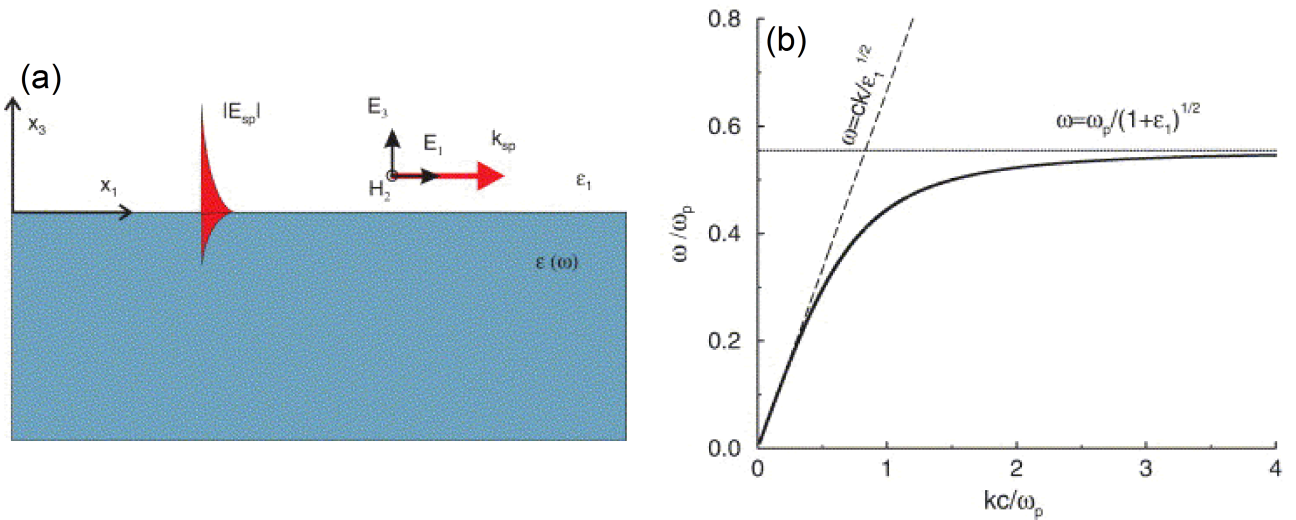


Figure 1.2: (a) Schematic representation of the system considered for analytical purposes. The SP is propagating along the x direction with a momentum vector  $k_{SP}$ . The electric field has components both along x and z directions, while the magnetic field only has component in the y direction. (b) Dispersion curve of an SP mode. The curve for the SP remains on the higher momentum side of the light-line, which means for any excitation with light, the momentum mismatch has to be taken care of. Figure adapted from Ref.[42].

When a surface plasmon interacts with a photon to form a propagating excitation, it is called a surface plasmon polariton. Such an excitation can be generated in metallic films or extended metallic nanostructures such as nanowires or nanoplates, by exciting a defect such as terminating ends, kinks or fractures. For sake of simplicity of theory, consider a metal (dielectric constant  $\epsilon_m$ ) dielectric ( $\epsilon_d$  with  $\text{Im}(\epsilon_d) = 0$ ) interface. Figure 1.2(a) shows a schematic of the

system. The electric field along x direction on the metal-dielectric interface can be given by [43]:

$$E_{SP}(x, z) = E_0 e^{ik_{SP}x - k_z|z|} \quad (1.4)$$

This represents a wave which is propagating along the x-direction with a wavevector  $k_{SP}$  and decaying perpendicular to the field (in the z-direction) with a decay constant  $k_z$ . The dispersion relation of the SPP is given by [43]:

$$k_{SP}^2 = \left(\frac{\omega}{c}\right)^2 \frac{\epsilon_d \epsilon_m}{\epsilon_d + \epsilon_m} \quad (1.5)$$

Figure 1.2(b) shows the dispersion relation of the SPP with respect to the light line. Since the SPP dispersion curve is in the part of the diagram below the light line (i.e.  $k_{SPP} > k_{light}$  for all  $\omega$ ), SPPs cannot be excited using direct illumination methods, or cannot radiate light. This can only happen at defects and grain boundaries, where symmetry breaking allows us to excite SPPs or allows SPPs to out-couple as photons from the metal due to the momentum-matching condition being met at such defects.

Owing to the fact that the SPP is confined close to the metal surface, depending on the combination of the metal and the dielectric surrounding it, there can be huge field enhancements in the vicinity of the metal film (or nanostructure). In case of a silver film in air illuminated by a red laser, this enhancement  $|E_{SP}|^2/|E_{light}|^2$ , where  $E_{light}$  is the incident field, can be more than two orders of magnitude [43]. Such large field enhancements can be put to use for various applications such as Fabry-Perot resonators [17], confining light emission in particular directions [20], remote excitation SERS [44], among others.

### SPPs in Ag nanowires

The system that supports SPPs that is important in context of this thesis is Ag nanowires, which have been synthesized by known polyol process [45, 46]. These wires are single crystalline in nature with a pentatwinned cross-section. Typical lengths range from 5  $\mu\text{m}$  to 100s of  $\mu\text{m}$ , and cross-sectional diameters are about 200-400 nm. For such wires, one of the easiest ways to excite the SPP modes is to focus a laser (usually a 632.8 nm He-Ne laser) to a diffraction-limited spot on one of the ends of the wire.[24, 47] Due to a mismatch between the momentum of the incoming photons ( $k_{photon}$ ) and momentum of the SPP ( $k_{SPP}$ ), an additional  $\Delta k_{scattering}$  has to be provided by a suitable scattering mechanism so as to allow for such an excitation to be possible. This can happen in a case where the laser is being incident on one end of the wire, where due to spatial symmetry breaking, such a momentum mismatch can be corrected for, and the photons can excite the SPP mode. This does not, however, happen when the laser is incident onto the center of the wire, where due to axial symmetry of the wire, the light cannot scatter axially, and thus cannot excite the SPP.[47]

Since the symmetry is pentagonal, analytically solving for the modes supported by the wire



is extremely difficult. However, a nice computational treatment has been given in Refs.[24] and [48]. Here, they use Finite Element Method (FEM) and Green's Dyadic method based calculations to solve for the modes of the pentatwinned silver nanowires. When the wire is free-standing, with only one kind of dielectric medium around it, the wire exhibits five corner modes which resemble the electronic modes of a molecule with  $D_{5h}$  symmetry [48, 24]. Any guided mode in this system is a linear superposition of these 5 corner modes. If the system is made more realistic, with the wire placed onto a glass substrate (as is usually the case in experiments), the symmetry now reduces from  $D_{5h}$  to  $C_{2v}$ , and supports 3 modes. One of these modes is a bound mode, with the electric field confined to the glass side, while the two other modes are leaky modes. Such theoretical and computational analysis is important to extract more physics out of the experimental results, as it reveals the fundamental mechanism about why a particular observation is seen in an experiment. This thesis therefore tries to touch upon certain aspects of the experimental results from a computational angle to probe the underlying mechanism involved.

### 1.1.3 Gap and cavity plasmons

Another category of plasmons, which is prevalently seen in metal-insulator-metal (MIM) type configurations is the so-called "gap plasmons". When the shape and the dimensions of the gap or the cavity are properly tuned, the field localization due to the two metal structures (which can be nanoparticles or waveguides) leads to enhancements in the fields up to 3-4 orders of magnitude.[49] Such gaps or grooves support various kinds of modes, which include gap-surface plasmons (GSPs) and channeled plasmon polaritons (CPPs). [50] If the dimensions of the nanoparticle in question are small, the gap plasmons can be highly confined and non-propagating, as in the case of "hot-spots" in bow-tie structures [7] or gold nanoparticles brought in close proximity to each other.[51] Such localization and enhancement of field is extremely important for SEFS or SERS measurements, as enhanced electric fields lead to enhanced emission from the molecules.[39] Extended cavities, such as the one considered here between the Ag wire and Au film, also support guided cavity modes, which are important in terms of nano-focusing and communications. Thus, such systems have to be studied in greater detail in order to get more control and understanding about the mechanisms involved.

## 1.2 Antenna parameters

Coming back to the original problem of antennas, there are certain basics that need to be studied in order to understand antennas better. The main function of an optical antenna is to allow an efficient interchange between the free radiation field and the emission by localized sources such as molecules and quantum dots.[4] This is a two way process, and antennas act both on the transmitting end (enhancing and directing the emission of the quantum emitter) and receiving

end (focusing free radiation onto the quantum emitter for enhanced local electric field). Figure 1.3 shows how an antenna structure can act in the transmission mode and receiving mode.

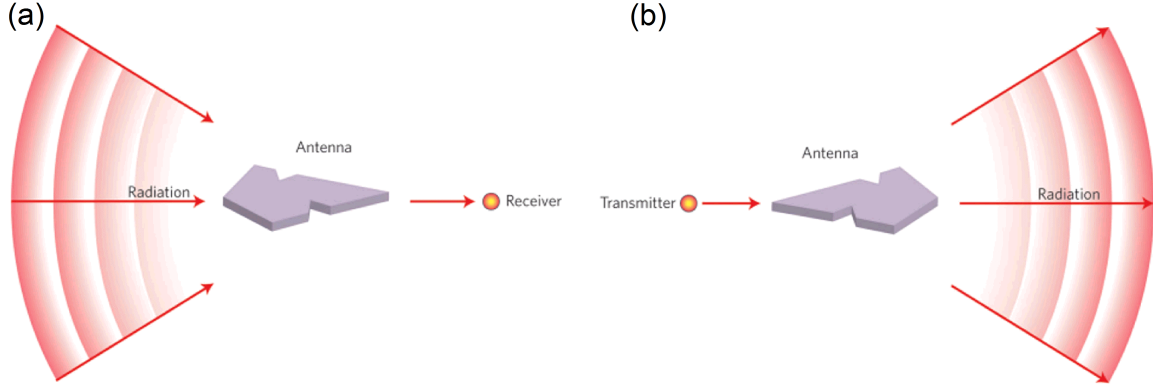


Figure 1.3: Antenna structure being used in (a) receiving mode and (b) transmitting mode. The arrows indicate the direction of energy flow. Usually the same structure is used both to channel free radiation onto a received, and to transmit the radiation from an emitter to the far-field. Figure adapted from Ref.[4].

Since there are two parameters that we talk about, namely enhancement and directivity, it is possible to parametrize an antenna in terms of these two quantities. Due to reciprocity, what we talk about in the transmitting geometry can be applied directly to the receiving geometry as well.[4] Thus, for now, let us consider only the transmitting geometry. As the antenna has been put in place to increase the efficiency of transmission of the quantum emitter, the antenna efficiency is a good parameter for measuring the enhancement: [4]

$$\epsilon_{antenna} = \frac{P_{rad}}{P_{tot}} = \frac{P_{rad}}{P_{rad} + P_{loss}} \quad (1.6)$$

Here,  $P_{tot}$  is the total power dissipated by the antenna,  $P_{rad}$  is the radiation power transmitted by the antenna, and  $P_{loss}$  is the power dissipated by antenna as heat or by other non-radiative mechanisms.

The directivity of an antenna defines how the antenna shapes the transmission and directs it towards the receiving body. This can be parametrized as: [4]

$$D(\theta, \phi) = \frac{4\pi}{P_{rad}} p(\theta, \phi) \quad (1.7)$$

where  $\theta$  and  $\phi$  are the angles in the direction of observation, and  $p(\theta, \phi)$  is the angular power density. The combination of the antenna efficiency and the directivity then gives us the gain factor  $G$ :

$$G = \frac{4\pi}{P} p(\theta, \phi) = \epsilon_{antenna} D \quad (1.8)$$

One more important parameter is the antenna aperture, which is equivalent to the absorption cross-section. If a receiver with a cross-section  $\sigma_0$  in vacuum is coupled to the antenna, the incident field  $E_0$  is enhanced to  $E$  at the receiver location, and the cross-section of the antenna aperture is given by:

$$\sigma = \sigma_0 \frac{|E|^2}{|E_0|^2} \quad (1.9)$$

Note that this is for the simplest case where the receiver is aligned with the electric field. In a general case, one has to take the component of the electric field along the receiver dipole axis. Nevertheless, studies have shown intensity enhancements of 4-6 orders of magnitude when antenna structures were used.[4] Antennas can thus very efficiently direct the free space radiation towards the receivers, enhance the field at the receiver location, and transmit the emission by the emitters back to the free space with very high efficiencies.

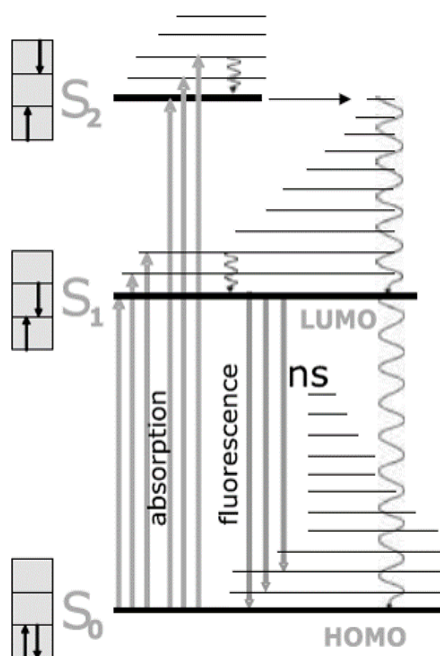


Figure 1.4: Energy level diagram of a typical molecule used in fluorescence experiments.  $S_0, S_1, S_2$  are singlet electronic states and have multiple vibrational states associated with each of them. Electrons that get excited due to absorption first return to the ground vibrational state for the particular electronic level, following which it can either return to the ground state radiatively (fluorescence) or non-radiatively (through heat dissipation). The radiative decay need not end at the vibrational ground state of the  $S_0$  state, and this leads to red-shifted photons being observed in the spectrum. Figure adapted from Ref.[26].

### 1.3 Molecular Emissions and Scattering processes

An important part of light-matter interaction is the interaction of light with molecules. This includes absorption of the light and reemission as fluorescence, phosphorescence or scattering

processes such as Rayleigh scattering and Raman scattering. This section deals primarily with fluorescence and Raman scattering, as these two processes, and the effects of coupling to metal nanoparticles on these processes, have been studied using experiments in the thesis in Chapter 3.

### 1.3.1 Fluorescence

In case of organic molecules, the transition between the HOMO (Highest Occupied Molecular Orbital) and the LUMO (Lowest Unoccupied Molecular Orbital) is the lowest energy electronic transition. Due to these molecules being multi-atomic systems, there are also multiple vibrational states that are superimposed onto these electronic transitions. Figure 1.4 shows the various states that we need to consider in case of fluorescence. The pumping of the fluorescent molecules is usually done by the resonant wavelength, which corresponds to one of the electronic transitions. This takes the electrons of the molecule to the LUMO, and this excited state typically has a lifetime of 1-10 ns.[26] The strength of such a transition is determined by the transition matrix element of the system between the HOMO and the LUMO. Once in the excited state, there are multiple pathways for the electrons to come back to the ground state. This can happen radiatively, through photons, or non-radiatively, through phonons. The radiative decay is known as fluorescence. Fluorescence is a spontaneous emission process. The quantum efficiency  $Q$  of the molecule gives the ratio of the radiative decay rate to the total decay rate: [26]

$$Q = \frac{k_r}{k_r + k_{nr}} \quad (1.10)$$

where  $k_r$  is the radiative decay rate and  $k_{nr}$  is the non-radiative decay rate. The interplay between vibronic states and electronic states is what determines how strong the fluorescence will be from a particular molecule. Strong fluorescence is observed mainly in cases of molecules which have a lower number of vibronic states, as that reduces the non-radiative pathways for the electrons to decay back to the ground state. Such molecules are typically known as dyes or fluorophores.

When such molecules are placed in the vicinity of plasmonic structures or cavities, the fluorescence is greatly enhanced due to what is known as Purcell effect. This happens due to a change in the environment of the molecule, which increases the probability of the excited electrons to follow the radiative decay rather than the non-radiative pathway.[52] In case of molecules in a cavity, this enhancement factor is given by: [53]

$$P = \frac{3}{4\pi^2} \left( \frac{\lambda}{n} \right)^3 \frac{Q}{V} \quad (1.11)$$

where  $P$  is the Purcell Enhancement factor,  $(\lambda/n)$  is the wavelength inside the cavity with a refractive index  $n$ ,  $Q$  here is the quality factor of the cavity and  $V$  is the mode volume of the

cavity. The reason for such a relation is that the local density of states at particular wavelength inside the cavity is modified according to the quality factor and the mode volume of the cavity, and since the local density of states determines how the molecule will decay back to the ground state, the fluorescence is enhanced due to this change.[53]

### 1.3.2 Raman scattering

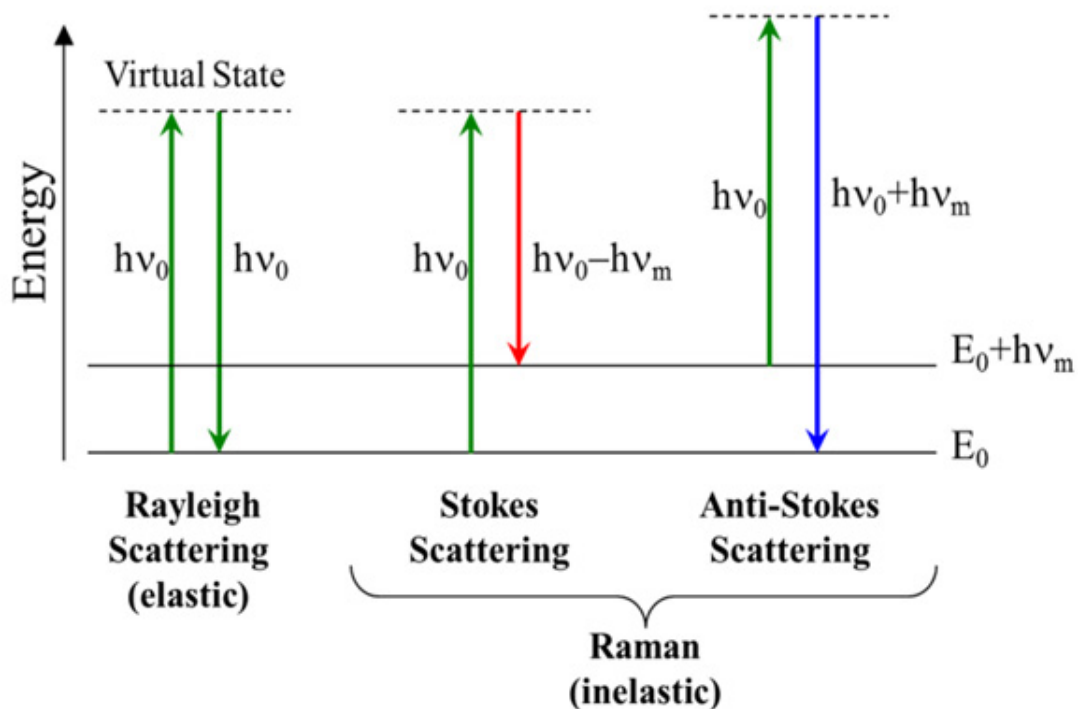


Figure 1.5: Scattering phenomena in a molecule. When the light scatters off an electron, it first takes the electron to a virtual state. This is followed by the electron coming back to the original state (Rayleigh scattering), absorb a quantum of energy and return to an excited vibrational state (Stokes scattering) or give a quantum of energy and return to a lower vibrational state (Anti-Stokes scattering). Figure adapted from Ref.[54]

Another way light interacts with molecules is through Raman scattering. Raman scattering is an important interaction that a molecule has with the incoming radiation, mainly because the peaks are extremely specific to the molecule in questions, and therefore the Raman spectrum of a molecule is a clear signature of the molecule being detected.[55] In this process, the light interacts with an electron from the molecule and takes it to a virtual state. In case of non-resonant Raman scattering, this transition is not one of the electronic transitions of the molecule, and so this "virtual state" is extremely short lived (hence the designation of scattering). The electron can now directly return to its previous ground state (known as Rayleigh scattering), or interact with the vibrational states of the molecule's ground state to give Raman scattering. If the electron comes back to a higher vibrational state of the molecule, the photon that scatters from it

is red-shifted, and the process is known as Stokes shift. If the electron comes back to a lower vibrational state, the photon gains a quantum of vibrational energy and is anti-Stokes shifted. Figure 1.5 shows schematically the three processes described here.

Now, if the incoming radiation has a frequency which matches one of the electronic transitions of the molecule, we get what is known as resonant Raman scattering. Here, the molecule goes to the excited electronic state, and may exhibit either fluorescence or Raman scattering. The two processes now compete, but in usual cases, the cross section for Raman scattering can be up to  $10^{14}$  times smaller than those of fluorescence.[26] To overcome this issue, one takes help of a technique known as Surface Enhanced Raman Spectroscopy, or SERS.

### Surface Enhanced Raman Spectroscopy

As the name suggests, the technique of SERS employs enhancement of Raman signals of molecules by enhancing the signal using tailored surfaces. This involves bringing the molecules into close contact of the surface, which interacts with the molecule and through specific processes, enhances the Raman signal intensity by up to 14 orders of magnitude.[56] This enhancement is a result of two mechanisms, electromagnetic and chemical.[39] Electromagnetic enhancement is the result of enhanced electric fields on the surfaces of metal films or nanostructures which result in large enhancements in the Raman intensities, while chemical enhancements are seen due to specific electronic interactions between the molecule and the surface to which the molecule gets adsorbed. Usually, the electromagnetic enhancement is extremely large as compared to chemical enhancement ( $10^{12}$  vs  $10^2$ ).[57]

The electromagnetic enhancement has been attributed to the local field enhancement that is observed due to plasmon generation on metallic surfaces. The enhancement goes as  $E^4$  [39, 58, 57, 41] where first two powers of  $E$  are due to the enhancement of the local electric field as felt by the molecule, while the other two powers of  $E$  are due to the enhancement of the Raman signals emitted by the molecule due to the antenna effects of the metal nanostructures. [41] A rigorous proof of this dependence is given in Ref.[58]. Note that since the Raman shifted photons are of a different frequency than the incident field, the enhancement should actually be written as  $E_{incident}^2 E_{Raman}^2$ , and so the resonant enhancement only occurs for a small window of wavelengths.[39]

In case of extended sources, such as silver nanowires, the two contributions to the enhancement factor are not equal. For the case of silver wire with silver nanoparticle attached to it, the local electric field goes as  $|E_{loc}(\omega, \theta)| = |E_0(\omega)| \cos \theta$  [41] where  $E_0(\omega)$  is the maximum local electric field obtainable at  $\omega$  which is the incoming laser frequency.  $\theta$  is the angle of polarization of the laser beam with the wire axis. However, the direction of the induced electric field is  $\theta$  independent. Thus the overall enhancement factor goes as [41]

$$\begin{aligned} G_{cavity} &\approx |E_0|^2 \cos^2 \theta \times |E_0|^2 \\ &\approx |E_0|^4 \cos^2 \theta \end{aligned} \tag{1.12}$$

Here we have assumed that the frequencies for the local electric field and the induced electric field (which leads to the Raman enhancement contribution) are approximately the same, which is true for small shifts. Note that depending on the direction in which the field is maximum depends on how the field is localized in the system. This may introduce a phase in the  $\cos^2\theta$  term, but the trend remains the same. For example, in the case of Ag wire on Au film, the enhancement is maximum perpendicular to the wire axis due to huge localization of the field. In this case, when  $\theta$  is defined with zero along the wire axis, the factor actually goes as  $\sin\theta$ .

The second mechanism for SERS is the chemical enhancement. In these kind of interactions, chemisorption of the molecule onto the substrate leads to new electronic states which act as intermediates to the Raman scattering. For example, many molecules chosen for SERS studies have their lowest electronic excitation in the UV region (but close to the visible range).[39] When these molecules are brought in contact with metal films, it is generally the case that the metallic Fermi energy is at about half of the HOMO and the LUMO of the molecule. Thus, charge transfer processes can occur between the molecule and the film lead to the excitations coming to the visible region. This leads to the Raman scattering becoming resonant with the incoming radiation, thereby enhancing the process.

In conclusion, SERS is a complex process with an interplay between electromagnetic and chemical enhancements. This process has been extensively studied for over three decades now[39, 41] and yet it is used extensively for various studies even now.

## 1.4 Definition and Motivation of Thesis problem

From the topics introduced above it can be seen that the antenna effects that metal nanoparticles have on molecular emissions are an interesting topic to study, not only for the academic value of it, but also for important applications like label-free detection of molecules. It is also a very important topic when looked at from the perspective of engineering of optical emission at the nano-scale. It is therefore imperative to identify and study systems which can lead to high Raman or fluorescence enhancements, and also give us some control over the directivity of the emission.

Many systems have been studied for such applications. For example, antenna effects of gold nanorods [22, 21] and coupled systems of gold nanorods such as Yagi Uda antenna structure [6] have been shown in literature. Such systems demonstrate that the plasmonic properties of such nanorods lead to strong enhancement of molecular emission in their vicinity. This effect is known as Surface enhanced Fluorescence. The emission is not only modified in terms of intensity but also in terms of direction of emission, and hence such nanorods can be utilized to direct photons from the molecular emission into particular directions. However, most of the work done in this area has been for the case of fluorescence. The system of gold nanorods has not been extensively studied for its Raman antenna effects, and hence it is important to study the system in this aspect. As mentioned previously, Raman spectrum of a molecule is

characteristic of that particular molecule, and thus is extensively used as a tool for chemical and biological analysis. Thus, gaining more understanding and control over the process is extremely important for further applications. The process also gives insight about the underlying plasmonic interactions between the components in the picture, and thus the SERS antenna effects can act as an indirect probe into the physics. One system for studying has thus been chosen to be gold nanorods over bare metallic film, which will be explained in more detail in Section 3.1 in Chapter 3.

The system described above deals with a single metal nanostructure placed on a metal film, and the experiments related to this system will probe the localized plasmonic effects and their interactions with the molecules in their vicinity. However, one can go further and ask the questions: what if a metallic waveguide, like a metal nanowire, is put into contact with a bare metal film? How will the propagating components of the plasmon behave? What interesting effects will we observe in the cavity? The system here, that is a silver nanowire on a gold film, is quite similar to gold nanorods over gold film. However, an important distinction between the two systems is the length dimensions of the nanostructure: the gold nanorods used are about 300-500 nm long and 20 nm thick, while the Ag nanowires used are 5-10 microns long and 200-250 nm in diameter. This implies that the plasmonic properties of the nanowires will surely be different as compared to the gold nanorods, as properties change with size in the nano regime. The quasi 0D hot-spot in case of a nanorod will in case of a nanowire be a quasi 1D "hot-line", or a series of hot-spots. Thus, it is a worthwhile investigation to do, as many questions are unanswered about this system even in the literature. There has been some research about the SERS properties of a nanowire particle junction [44], and investigation about the cavity enhancement has been done in some detail [59]. However, basic properties such as field profiles inside such a unique cavity, how the system will behave when excited at various locations, the polarization dependence of the SERS signal from molecules placed inside the nanowire-on-mirror cavity system, dependence of input and output polarization, effects due to dielectric spacer, input power dependence, etc. have not been studied in detail in the literature, and therefore need to be studied to understand the full scope of the coupling effects and the cavity effects of such a hybrid system. Section 3.2 in Chapter 3 details the experiments done on Ag nanowire-on-mirror system, while Chapter 4 mainly addresses the simulation aspects of the study in greater detail.



## Chapter 2

# Synthesis of Symmetric and Asymmetric Gold Nanoparticles

An important requirement in doing experiments in nano-photonics and plasmonics is the fabrication or wet-synthesis of nanostructures necessary to probe the desired effects. For example, it is known that gold nanotriangles or triangular nanoprisms show quadrupolar moments [60, 61, 62]. These particles also show high field enhancements near their corners, mainly due to LSP (localized surface plasmons) excitations and lightning rod effect at the corners [60] which also lead to third-order nonlinear effects [62]. Gold nanorods have been of quite some interest due to their inherent anisotropic nature, observation of PL (photoluminescence) [63], TPL (two photon luminescence) [64, 65, 66, 67], and SHG (second harmonic generation) [68], and observation of interesting antenna effects that change the emission properties of molecules in their vicinity [21]. Gold nanospheres, even if they are isotropic in nature, have a thinner coating of capping agents on the surface as compared to other gold nanostructures, and as such, lead to huge SERS signals when a Raman active molecule is brought in the vicinity of these particles. Such large surface enhancements have been used for medical uses such as cancer diagnostics[19]. Nanospheres can also be arranged neatly onto 2D substrates with large-range order, leading to interesting properties in their resonances [69].

Thus, fabrication or wet-synthesis of such structures becomes an important part of research. Various techniques have been used to form structures of desired shape and size. Three of the most common techniques are Lithography-based fabrication, Chemical vapor deposition (CVD), and wet synthesis. Lithography based methods (photolithography, electron-beam lithography) are extremely precise and can be used to create desired geometries with extremely well-defined parameters. However, these methods are tedious and require sophisticated instrumentation. These methods also lead to polycrystalline nanostructures, which cause issues such as grain defects. CVD based techniques, while being able to produce extremely high quality nanostructures, require sophisticated instrumentation such as high vacuum facilities and ultra-clean environments. Wet-synthesis techniques, on the other hand, lead to monocrystalline

structures and do not require any special instruments. Such methods can easily be used at room temperature in normal lab environment, and are therefore much more straightforward to use. There is also versatility in these methods due to a wide variety of shapes and sizes of nanoparticles that can be produced, as well as the materials that can be used to produce such particles. The following sections detail the methods to synthesize gold nanospheres, gold nanotriangles, and gold nanorods using wet-synthesis methods.

## 2.1 Synthesis of Gold nanospheres

Spherical gold nanoparticles were prepared using citrate reduction method as given in literature [70]. DI water was added to 625  $\mu$ l of 20 mM HAuCl<sub>4</sub> (Sigma Aldrich, 99.9%) to make a final volume of 50 ml. The mixture was heated to 100° Celcius. 0.3 ml of 1% solution (w/v) of Sodium citrate in DI water was added to the boiling solution of HAuCl<sub>4</sub>. The solution was let to boil for an hour while maintaining the volume, and then was let to cool till room temperature. The resulting solution was a deep magenta color, with monodisperse Au nanospheres of about 65 nm diameter. Figure 2.1(a) shows the SEM image of the Au nanospheres while Figure 2.1(b) shows the UV-Vis spectrum of the solution. The peak position indicates the size of the particles [70] as the surface plasmon resonance (SPR) shifts to higher wavelength as the diameter increases.

Since these particles have a very thin capping of citrate molecules, they can be used for SERS applications. These particles were thus used for one such application, wherein they were arranged in a V shaped antenna structure using surface modification and EBL patterning, and the antenna effects of such a structure on SERS signal from Nile Blue were studied. The work related to the arrangements of these nanospheres was done primarily by Dr. Debrina Jana.

## 2.2 Synthesis of Gold nanotriangles

Multiple methods were tried for synthesizing gold nanotriangles of reasonably large size (150 nm or above). However, most procedures only detail ways to produce nanotriangles or nanoprisms upto 120-140 nm edge length [62, 61, 71]. Also, yield of nanotriangles was extremely low for all procedures followed. Of these, the one pot synthesis method [71] gave decent yield upon some modification, and will be detailed here.

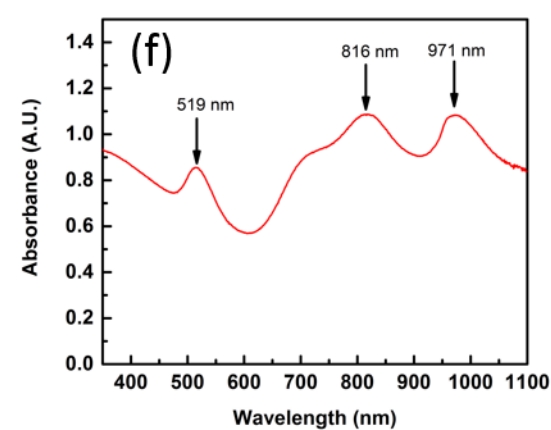
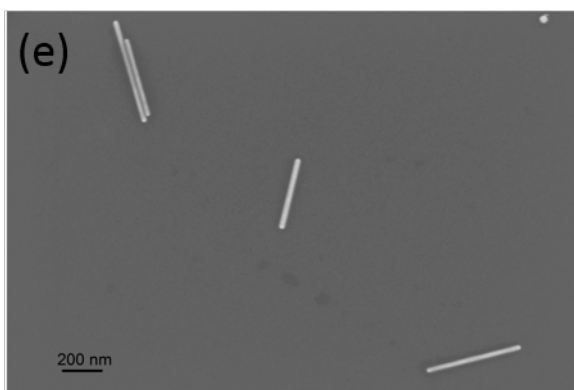
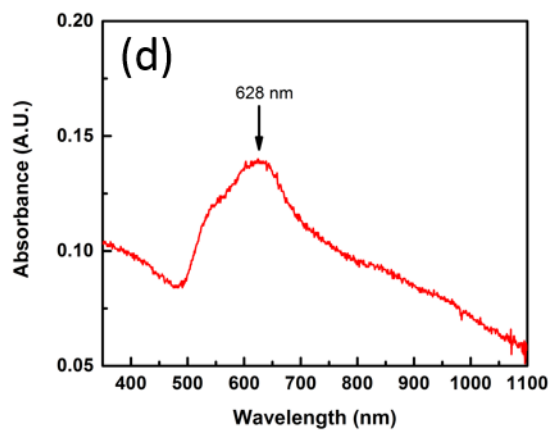
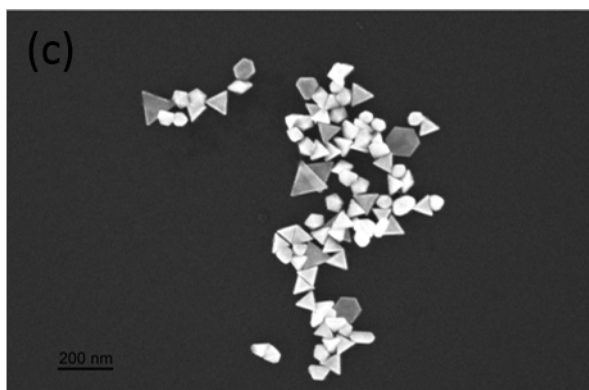
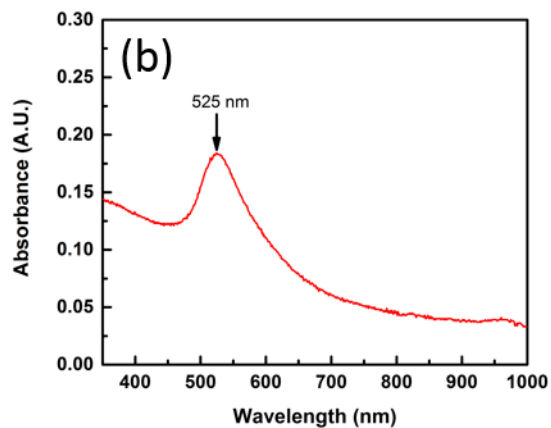
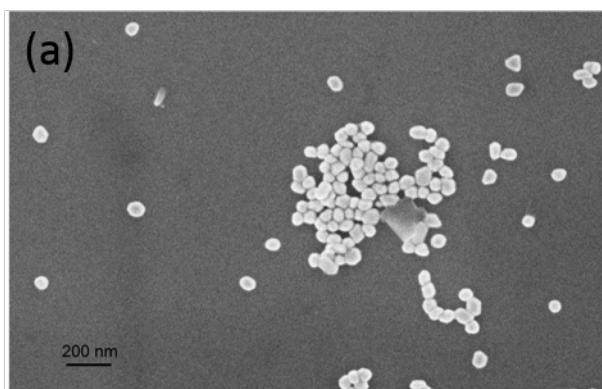


Figure 2.1: SEM images of synthesized nanoparticles (Au nanospheres(a), Au nanotriangles (c) and Au nanorods (e)) and UV-Vis spectra for nanoparticle solutions (Au nanospheres(b), Au nanotriangles(d) and Au nanorods(f))

1.6 ml of 0.1 M Hexadecyltrimethylammonium chloride (CTAC, Sigma Aldrich,  $\geq 98\%$ ) solution was mixed with 8 ml DI water. 75  $\mu\text{l}$  of 0.01 M KI was added to it, followed by addition of 80  $\mu\text{l}$  25.4 mM  $\text{HAuCl}_4$  and 20.3  $\mu\text{l}$  of 0.05 M NaOH (the original paper uses 0.1 M NaOH, however 0.05 M NaOH leads to larger edge length). While shaking the solution, 80  $\mu\text{l}$  of 0.064 M Ascorbic Acid was added to the solution, followed quickly by addition of 10  $\mu\text{l}$  of 0.05 M NaOH. The solution was shaken for a few seconds and left to rest. The solution becomes blue in colour, indicating formation of gold nanotriangles. Triangles were then purified by centrifugation at 4000 rpm for 15 minutes, followed by redispersion of precipitate in DI water, again followed by centrifugation and redispersion in DI water. This was done to clean the excess CTAC from the solution as well as to remove extremely small Au particles that may have formed in the process. Figure 2.1(c) shows the SEM image for the Au nanotriangles formed using this method, while Figure 2.1(d) shows the UV-Vis spectrum for the triangles. This spectrum matches with the UV-Vis spectrum given in the original paper [71].

Even though triangles were formed, the variation in edge-length was large (70nm to 130nm). The maximum edge length was also quite small for it to be possible to identify single nanoparticle using dark-field microscopy. Hence these particles were not used for any further experiments.

## 2.3 Synthesis of Gold nanorods

There are various methods available in literature [72] for synthesis of Au nanorods of various aspect ratios and lengths. All of these procedures are seed mediated, and how one prepares the seed has implications on what the length and the aspect ratio of the final rods will be. The method followed here leads to a 3.5 nm sized citrate stabilized seeds, and leads to 300-500 nm long and 20-25 nm thick cylindrical gold rods. The procedure involves a 4 solution process. The first solution is the seed solution, while the other 3 are the growth solutions. For preparation of the seed solution, 20 ml of aqueous solution with  $2.5 \times 10^{-4}\text{M}$   $\text{HAuCl}_4$  and  $2.5 \times 10^{-4}\text{M}$  trisodium citrate. To reduce the gold, 0.6 ml of ice cold aqueous solution of 0.1 M  $\text{NaBH}_4$  was added to it while stirring. The solution turned orange-red which is due to the formation of 3.5 nm sized seed particles [72].

For the growth phase, 3 solutions A, B and C were prepared. Solutions A and B were made using 9 ml  $2.5 \times 10^{-4}\text{M}$   $\text{HAuCl}_4$  and 0.1M CTAB. 50  $\mu\text{l}$  of 0.1M Ascorbic acid was added to both A and B while stirring. This makes the solution change color from yellow to colorless. Solution C was made using 45 ml of  $2.5 \times 10^{-4}\text{M}$   $\text{HAuCl}_4$  and 0.1M CTAB. 250  $\mu\text{l}$  of 0.1M Ascorbic acid was added to this solution while stirring. To further proceed with the synthesis, 1 ml of seed solution was added to solution A while stirring. After 15 seconds, 1 ml of this mixture was added to solution B while stirring. After 30 seconds of resting time, 5 ml of this mixture was added to solution C while stirring, and then let to rest for 16 hours at room temperature. After 16 hours, the liquid on top, which was reddish-brown in color,

was removed slowly. At the bottom of the container, a dark-brownish precipitate was observed which was redispersed in DI water, followed by centrifugation at 5500 rpm for 15 minutes and redispersion to remove excess CTAB from the solution. The resulting solution showed a good yield of Au nanorods, as seen in Figure 2.1(e). Figure 2.1(f) shows the UV-Vis spectrum for the sample. The longitudinal resonance of the rods falls in the IR region [72], however, it is possible that the peaks seen in the UV-Vis arise due to the transverse resonance, and presence of impurities such as gold nanospheres and nanotriangles.

These rods were used for further experiments such as observation of SERS enhancement and to study polarization dependence, which will be explained in more detail in Chapter 3.

## Chapter 3

# Study of Antenna Effects of Asymmetric Metal Nanoparticles

As described previously in Chapter 1, large body of research exists on the antenna effect on fluorescent molecules of gold nanorods.[6, 22, 21] However, there is lack of research of this system in terms of its Raman antenna effects. Here we try to address this problem. To increase the Raman cross section of the molecule, a dye resonant at 632.8 nm excitation (Nile Blue, Figure 3.1) was chosen as an analyte. However, as we are trying to study a resonant dye with the same excitation wavelength, Raman scattering and fluorescence compete with each other. Furthermore, the nanorods that are being used for enhancement effects, by virtue of the synthesis method followed, have a coating of CTAB around them. Such a layer of CTAB prevents any molecule to come into direct contact with the metal, which does not quench the molecular fluorescence but in fact enhances it. Therefore to extract resonant Raman signal out of such a system is difficult. However, the Raman antenna effects of a slightly modified system can be studied by making a small change in the system: changing the substrate to a bare metallic film, or a metallic mirror. A bare metallic film will quench the fluorescence of the molecules that come into contact with it, and the emission of these molecules in the cavity between the metal film and a gold nanorod will be greatly enhanced due to high electric field intensity in such cavity, which is essentially a hot-spot. This system also creates image dipoles in the film, which enhance the field. This is only true for vertical dipoles, as horizontal dipoles are cancelled out due to the film.[73] This effect adds to the enhancement of tightly localized field[36], leading to extremely high electric fields and therefore high enhancement of the molecular emission. Thus this system simultaneously enhances the Raman signal due to electronic enhancement effect and quenches the fluorescence of the resonant dye, giving us the perfect system to study the Raman antenna effects at a single nanoparticle level. Section 3.1 addresses some of the issues regarding this system wherein gold nanorods have been coated with Nile Blue molecule, which is resonant at 632.8nm, and these rods have been placed on a bare gold film.

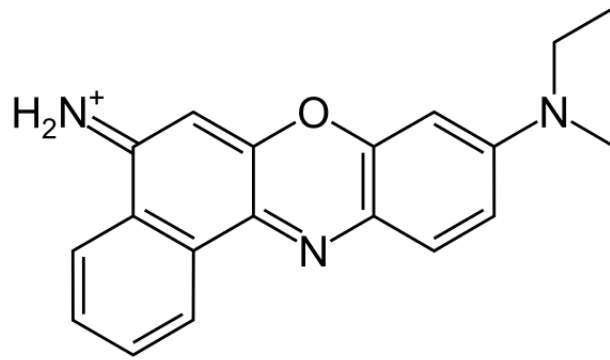


Figure 3.1: Molecular structure of Nile Blue molecule. The  $590\text{ cm}^{-1}$  Raman mode involves all atoms of the molecule, and cannot be attributed to a single bond. [74]

As previously mentioned in Chapter 1, the system of Au rods on Au film deals with LSPs generated in the Au rods. To study effects of SPPs on Raman enhancements, and to study how a 1D system behaves as a Raman antenna, the system of Ag nanowires on Au film was chosen. The system of a "hot-line" created between the wire and the film is extremely interesting, as it has not been studied in great detail and is sure to reveal new physics. Thus the section 3.2 details the experiments done in order to study this system and its properties as a Raman antenna in greater detail. (Chapter 4 deals extensively in looking at the problem of Ag wire on Au film from a simulations perspective, in order to understand the nature of plasmonic interaction between the wire and the film in detail.)

### 3.1 Optical studies of Au nanorods on Gold film

As mentioned before, the system we are probing here is a gold nanorod coupled to a metallic film, which in this case is a bare gold film. The bare gold film was coated on a glass coverslip using thermal evaporation method. The thickness of the film used was about 50-60 nm, the reason for which will be shortly discussed. The Au nanorods were mixed with a Nile Blue solution of concentration  $10^{-6}\text{M}$  and kept overnight, followed by dropcasting onto the gold film. Figure 3.2 shows the schematic of the system to be studied. One major problem faced during studies of single nanoparticles is locating a single nanoparticle using an optical microscope. To study such a system requires a method that can be coupled to an optical microscope which can point out possible candidates for study. As mentioned before, dark-field microscopy is such a technique, which is easy to handle in this scenario [28, 29, 31]. Of the various methods that are employed for dark-field microscopy, special dark field condensers require the microscopes to be of specific architectures to be able to be incorporated into the illumination profile. Waveguide scattering microscopy methods require precise illumination of the substrate, while large angle incidence works best with opaque substrates as it utilizes the backscattering of light from the nanoparticles. TIR based imaging techniques require a specially designed prism known as

Dove prism. In such a prism, the beam enters one of the transparent sides of this prism parallel to the top surface of the prism. This beam is refracted in such a way that it is incident on the top surface at an angle ( $\sim 76^\circ$ ) larger than the air-glass critical angle ( $\sim 42^\circ$ ). Thus, evanescent field is created in the vicinity of the top surface which quickly dies down [26]. If however, a nanoparticle comes in this field, it can couple to the field and scatter it to the far field, which can then be detected in the CCD. [33] The background does not scatter the light as the substrate used is smooth, and thus only the nanoparticles (and any defects in the substrate) are visible in the camera with high contrast. This is not a conclusive method to detect single nanoparticles, and has to be thus coupled to other techniques such as correlating using SEM or polarimetry to make sure that the scatterer being studied is indeed a single nanoparticle of our interest. However, this is a powerful technique, and has been employed here for imaging purposes.

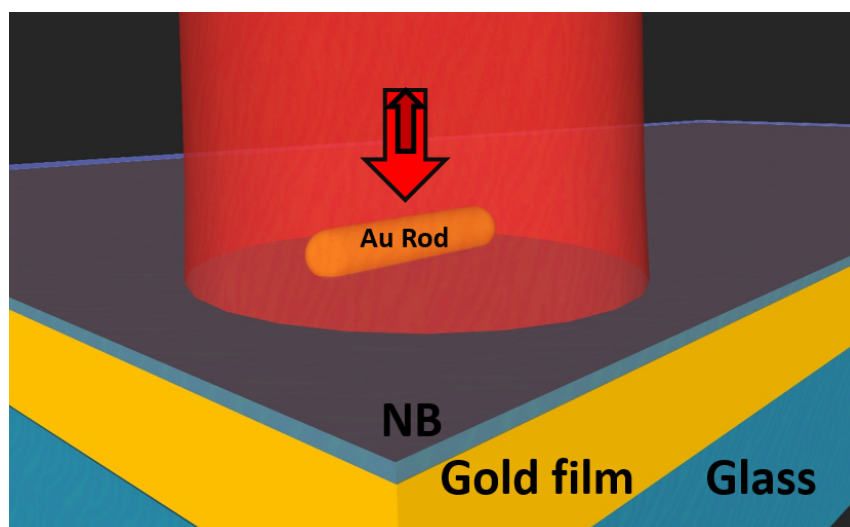


Figure 3.2: Schematic of the system to be studied. An Au rod was placed on an Au film with a coating of Nile Blue molecules. Excitation was done with 632.8 nm He-Ne laser, and spectrum was collected using setup given in Figure 3.3

### 3.1.1 Experimental setup and basic results

Figure 3.3 shows schematic of the microscopy and spectroscopy setup used for the purpose of studying the Raman antenna effects of single Au rods coated with NB and placed on a bare Au film. As previously mentioned, we used a Dove prism (N-BK7, refractive index = 1.52). The glass side of the gold-coated coverslip was coupled to the Dove prism using an optical index-matching oil. For the dark-field setup, white light supercontinuum laser (Fianium WhiteLase Micro) was shined through the Dove prism to set up TIR based dark-field illumination at the sample. For SERS measurement, commercially available confocal Raman spectrometer (LabRam HR) was used, and an internal 632.8 nm He-Ne laser was used to excite the nanorods. A  $\lambda/2$  plate was used to rotate the polarization of the excitation laser. A reflection based edge filter was used to avoid the excitation from entering the spectrometer. An objective



lens of 100X, 0.9 NA was used to collect the emission response of the molecules. Acquisition was done for 5 seconds. The results for various particles are given in Figure 3.4(a). The spectra show huge enhancement of Raman spectrum of the Nile blue molecule, with the  $590\text{ cm}^{-1}$  line being the most prominent. All the particles show the same spectrum, with varying enhancement. This variation in enhancement can be attributed to multiple things. It is possible that different lengths of the rod give different enhancement factors in the cavity, or the entity that was actually probed was not a nanorod but an impurity such as a nanosphere or an ensemble of particles. Thus, by looking at the Raman spectrum, it is not possible to guess whether the particle being probed is actually a nanorod or even whether it is a single particle or not. However, it is clear that there is enhancement of the Raman signal due to the system used here, and hence it can be said that the system is showing antenna effects at least in terms of the gain factor.

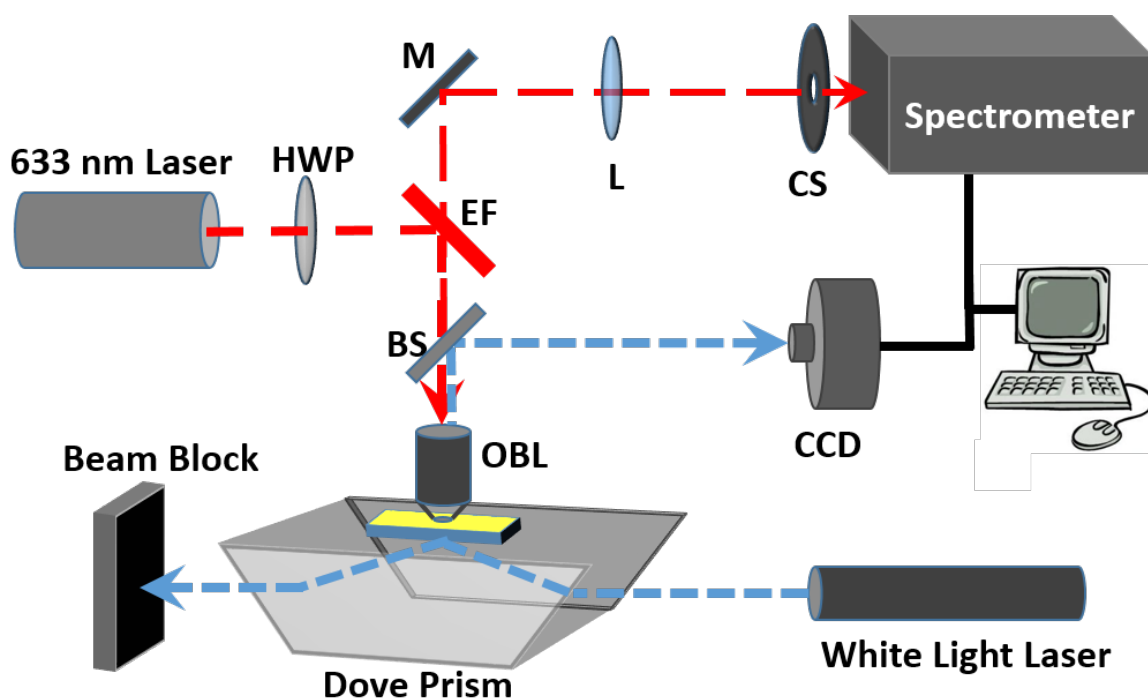


Figure 3.3: Schematic of the setup used for enhancement and polarization dependence measurements. The white light supercontinuum laser has been used only for dark field imaging purposes, and not for spectroscopy. OBL: Objective Lens; BS: Beam Splitter; EF: 632.8 nm Edge filter; HWP: Half Wave Plate; M: Mirror; L: Lens; CS: Confocal Slit; CCD: Charge Coupled Device

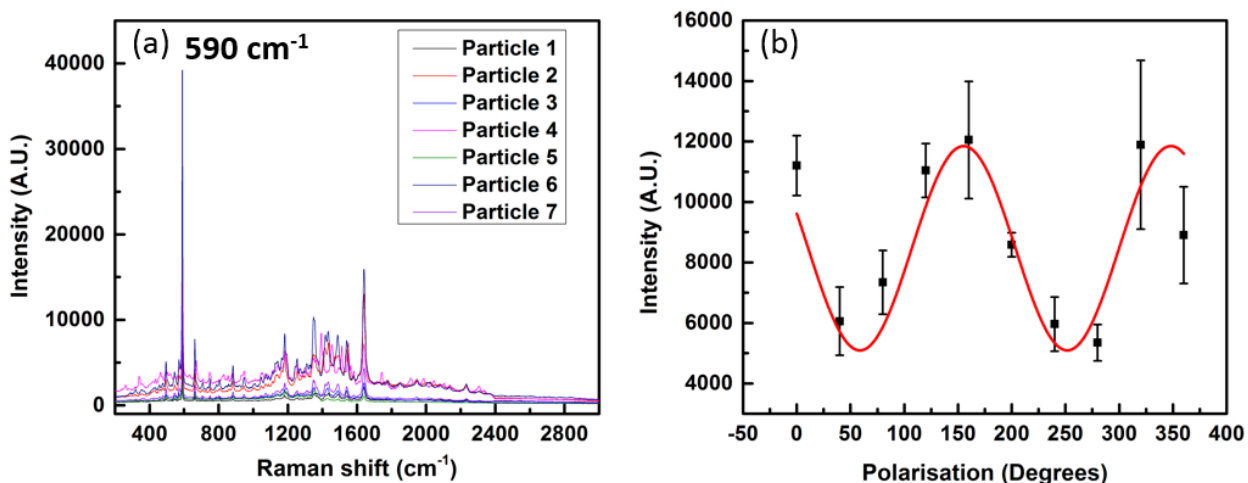


Figure 3.4: (a) Spectra as acquired from various particles observed using dark-field imaging. Clear signatures of Nile Blue spectrum are visible in the Raman spectra. The intensity shows that there is huge enhancement of Raman scattering due to large electric fields generated at the hot-spots between the film and the particles. (b) Polarization dependence of one particles observed. The fit is extremely poor, possibly due to the particle geometry actually not leading to a  $\cos^2\theta$  dependence of enhancement factor.

### 3.1.2 Polarization dependence of SERS signal

To further probe the antenna effects, input polarization dependent studies were done on multiple particles which were single particle candidates. The quantity to be measured was chosen to be the intensity of the signature  $590\text{ cm}^{-1}$  peak of the NB Raman spectrum. Figure 3.4(b) shows the plot of the  $590\text{ cm}^{-1}$  peak intensity vs input polarization angle for one such particle. As we see, there is some dependence on input polarization, but the fit is very poor (Adj.  $R^2$  value = 0.65). There are other issues in the measurement as well. Firstly, the peak intensity is not constant for multiple measurements of the same particle. In certain cases, the intensity varied by as much as 35000 counts. Such variation in intensity can be a result of multiple effects, such as diffusion of molecules from the modal volume or hot-spot which can be of thermal or non-thermal origins, or changes in molecular structure of the dye due to extremely intense electric fields in the hot spot.[55] However, most particles showed variations which were a few hundred or a few thousand counts, and such particles were studied for polarization dependence, since otherwise it would be extremely difficult to isolate the polarization effects from the inherent variation of the SERS. Another issue with the experiment is that there is no conclusive evidence that the particles under study are in fact single Au nanorods. Unless such a conclusion can be reached, one cannot be certain that the polarization dependence of the spectra observed is due to the plasmonic properties of the Au rod, or due to some complex properties of a system of Au particles.

### 3.1.3 Limitations

To overcome this issue, it was suggested that correlation using SEM be done on the particles being probed. For correlation, the address of a particle studied in the spectrometer has to be known by using grid like markings made on the gold film. Once the address is known, the sample can then be observed under SEM and by finding the exact address of the particle, and one can see if the particle that was studied was indeed a single Au nanorod, or an ensemble or other particles. However, there were multiple problems with this approach. Creating a grid onto a gold film is difficult as the adhesion of the materials used is a problem. Secondly, as the length scales in question are of the order of 300-500 nm, the grid has to have a resolution of that order which is a difficult task in terms of photolithographic resources available. This, combined with the issues in adhesion of the grid led to problems in correlation of the particles with the spectra acquired. Impurities were also a problem, as this meant that one could never be sure if a particular particle observed is definitely a rod. These issues could not be solved in the duration of the project, and hence no further data is available for this system as of now. However, efforts are under way to take this study further as these effects are extremely interesting and need to be probed thoroughly and systematically.

## 3.2 Optical studies of Ag nanowires on gold film

The previous set of experiments dealt with a quasi-0D metallic NP over a mirror system, and was aimed at studying the interaction between the two metallic objects. However, as the nanorods were extremely small in size (as compared to the wavelength involved and the spot size of the laser beam), only the localized surface plasmon properties could be probed. To probe the effects of an extended cavity system over a metallic mirror and how propagating plasmons interact with localized plasmons, the system of Ag nanowire over metallic mirror is an extremely good system to study. The Ag wires were synthesized using a known procedure [45, 46], and have a pentatwinned structure [75]. Figure 3.5 shows (a) an optical image as seen from a 100X objective lens and (b) an SEM image of a silver nanowire. The SEM image reveals the facets of these wires, which are in fact penta-twinned in nature. [76] Typical wire lengths used in the experiments are about 10-12 microns in length, while the diameters of the wire range between 300-500 nm. These wires have a coating of polyvinylpyrrolidone (PVP) of up to 5 nm on the sides. [76, 77] PVP is a dielectric in nature. Such a coating implies that any molecule which is placed in the vicinity of such a wire will not be in direct contact of the silver, but some distance away from it, thereby enhancing its fluorescence. To test this, Ag wires were coated with NB molecules and drop-casted onto a glass coverslip. Excitation was done with 632.8 nm He-Ne laser, and the signal was collected using a 100X 0.8 NA objective lens. Figure 3.6 shows the spectrum observed in this experiment. As expected, broad fluorescence peak is observed with a large intensity, which confirms the hypothesis made earlier. The Fabry-

Perot modes observed riding over the fluorescence peak are due to the reflection between two faces of the coverslip. Thus, it is difficult to extract any information about the Raman modes of the molecule in this setup. To observe the Raman antenna effects of a slightly modified system, however, is possible, by putting a bare gold film below the wires. The effects of such a system would be: a) the film will quench molecular fluorescence of the molecules that are in direct contact with the film b) the fields in the cavity between the wire and the film (which includes the dielectric layer of PVP) will be greatly enhanced due to confinement effects of the cavity and the mirror dipoles created in the film which will enhance the Raman signals of the NB molecules. Thus, this is a promising system to study how the Raman signals of the Nile blue molecule are modified in the presence of a plasmonic waveguide. Figure 3.7 shows the schematic of the system used for the following experiments. The silver wires were mixed with  $10^{-6}$ M NB, kept for some time, and then drop-casted onto a thermally deposited gold film. The gold film used was about 50-60 nm thick.

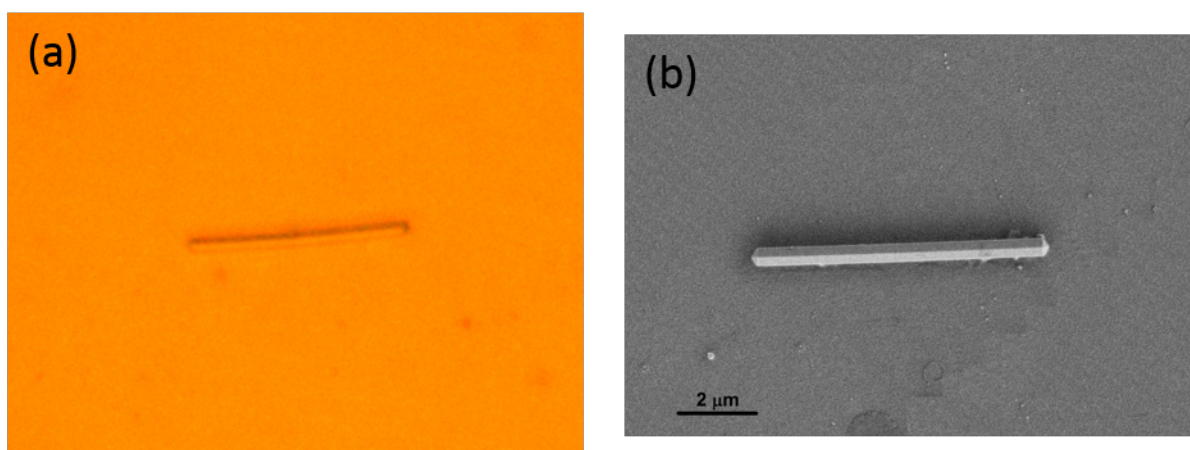


Figure 3.5: (a) Optical image as seen from a 100X 0.95 NA objective lens. The sample was illuminated through the lens using a white light source. (b) SEM image of a wire. The top facets of the penta-twinned wire can be clearly seen.

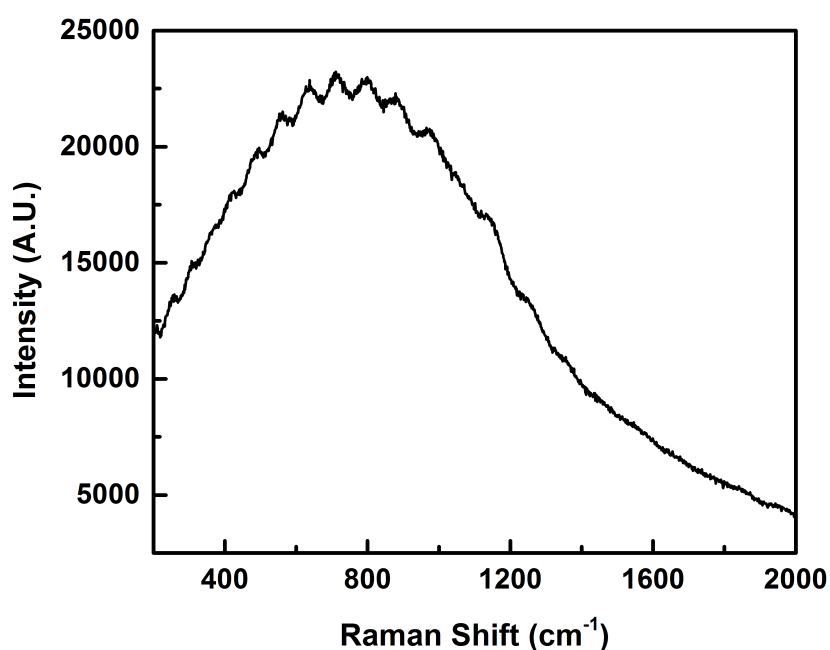


Figure 3.6: Fluorescence spectrum as observed for silver nanowire coated with Nile Blue and drop-casted over a glass surface. The wire was excited using a 632.8 nm He-Ne laser with a 100X 0.8 NA objective lens at the center with polarization perpendicular to the wire, and collection was done from the same point. Fabry-Perot modes are clearly seen, which are due to reflections between two sides of the glass coverslip used.

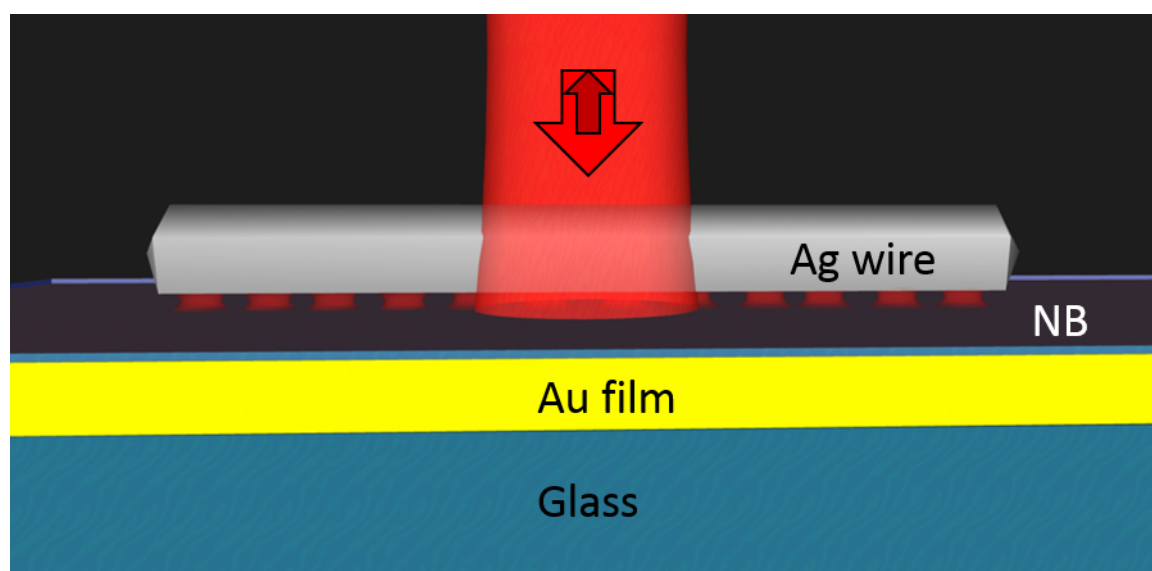


Figure 3.7: Schematic of the system used for experiments in the enhancement and polarization dependence experiments. The gold film is coated using thermal evaporation and has a thickness of 50-60 nm. Nile Blue was mixed with the wire and the mixture was drop-casted onto the film. The wire was excited at the center, and collection was done at the same point.

### 3.2.1 Enhancement and Polarization dependence of SERS signals

The spectrometry of the system in this experiment was done using LabRam HR confocal spectrometer. White light illumination was used to visualize Ag nanowires, as the large sizes of these wires implied that dark-field was not necessary for visualization. The objective lens used was 100X 0.8 NA, and the acquisition time was kept at 5 seconds for each of the measurements. Figure 3.8(a) shows the spectrum observed by exciting the center of a wire and collecting the spectrum from the same point. The spectrum clearly shows huge enhancement of the Raman modes of NB, while little to no fluorescence background. It is completely different from the spectrum seen for the plasmonic wire-on-glass system as seen in Figure 3.6, and hence we can say that the metallic mirror underneath the wire and the cavity between the wire and the film are having some effect onto the Nile Blue molecules in contact with it. The  $590\text{ cm}^{-1}$  line is the most intense mode that is observed, and that was selected for further analysis. In further experiments, it will be probed how the plasmonic wire-on-mirror system shows antenna effects for this particular mode of the NB Raman spectrum.

Figure 3.8(b) shows the input polarization dependence of the intensity of the  $590\text{ cm}^{-1}$  line. The angle is with respect to the axis of the wire. The polarization was changed using a  $\lambda/2$  plate on the input end of the spectrometer. The cos squared fit [41, 78] for the plot has an  $R^2$  value of 0.92, and so the fit is good, with a phase shift of  $90^\circ$  associated with the fit. Figure 3.8(c) shows the same data on a polar plot. As can be clearly seen from the two plots, the intensity of the  $590\text{ cm}^{-1}$  line is maximum when the input polarization is perpendicular to the the axis of the wire, while the minimum intensity is observed when the polarization is along the wire. One way to explain this would be to consider the maximum electric field in the system. As mentioned previously, SERS enhancement is proportional to  $|E_{max}|^4$  [41]. Thus if we look at the maximum electric field in each case, we could make a prediction about the SERS signal obtained from the system. From the observations, it can be hypothesized that when the field is along the wire, there is generation of propagating modes in the cavity between the wire and the metallic mirror. Such modes would lead to delocalization of the electric field along the wire. When the polarization is perpendicular to the wire, the field would be highly localized due to no propagating modes being generated. Thus, the maximum field intensity should be much higher for polarization perpendicular to the wire as compared to polarization along the wire, leading to higher SERS signals as the polarization is changed from along the wire to perpendicular to the wire.

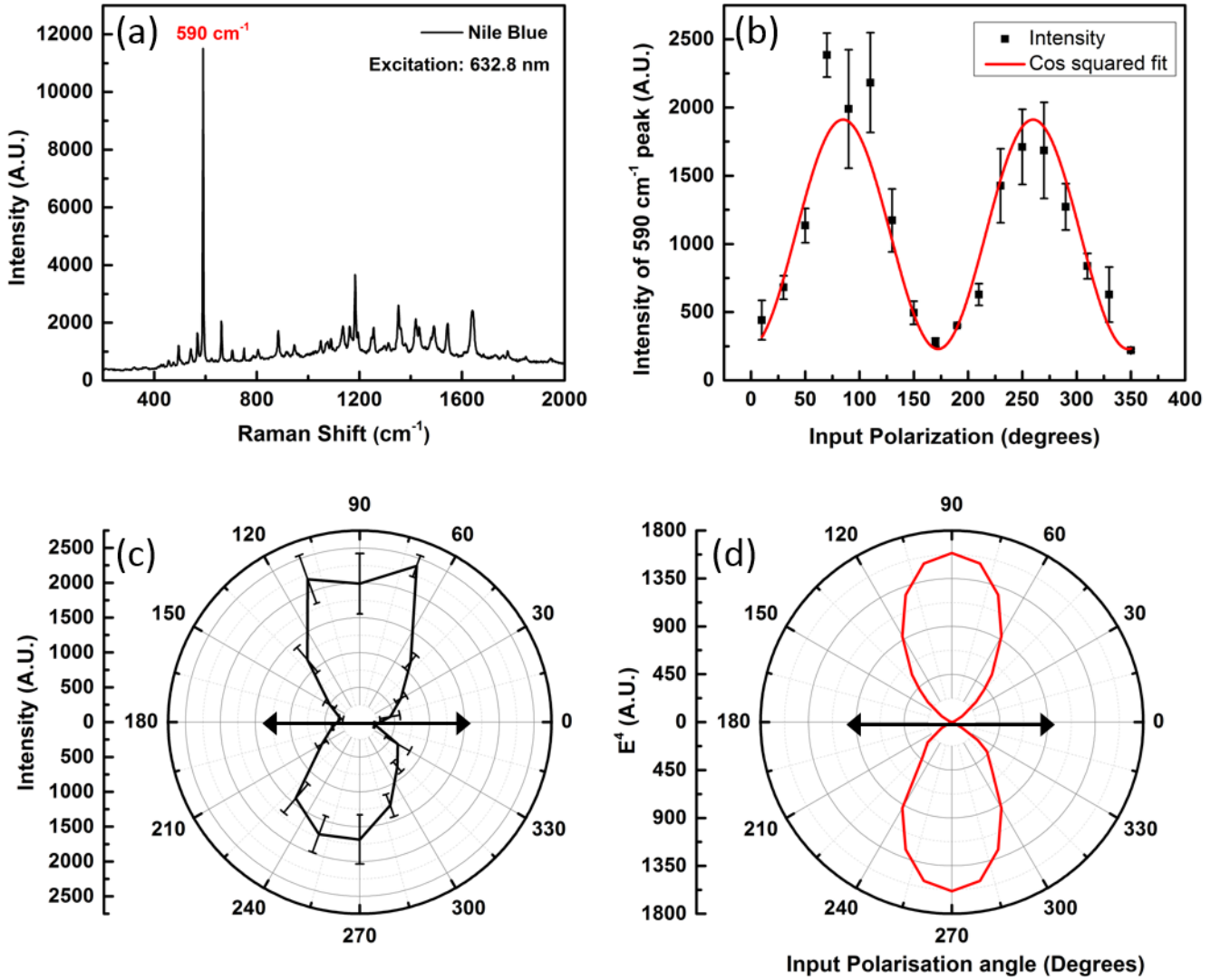


Figure 3.8: (a) Spectrum observed for system shown in Figure 3.7. Huge enhancement of the Raman signal of Nile Blue is observed due to electromagnetic pathway of enhancement. The  $590\text{ cm}^{-1}$  line is the most prominent mode observed and will be used for further experiments. (b) shows the input polarization dependence of the  $590\text{ cm}^{-1}$  line. The  $\cos^2\theta$  fit is good with  $R^2$  value of 0.92. (c) The polarization dependence of the  $590\text{ cm}^{-1}$  line on a polar plot. The arrows show the axis of the wire. A clear dipolar behavior can be seen, with maximum intensity perpendicular to the wire. (d) FEM simulation results for  $|E_{max}|^4$ . The arrows show the axis of the wire. The behavior matches with the experimental data.

To confirm this hypothesis, Finite element method (FEM) simulations were done (Chapter 4 will explain the simulations in higher detail) to estimate the polarization dependence of  $E_{max}$ . For an input power of 1W, it was observed that  $E_{max}$  when the polarization is along the wire is 1.53 V/m while  $E_{max}$  when the field is perpendicular to the wire is 25.09 V/m. There is clearly huge delocalization of the electric field when the field is along the wire. The field profile also shows propagating modes along the wire when the input field is along the wire, thus confirming

our hypothesis. Figure 3.8(d) shows the polar plot of  $|E_{max}|^4$  as a function of input polarization. The plot follows a cosine squared trend, and matches very well with the experimental observations. Thus, the polarization dependence of the SERS enhancement is extremely strong, and the output intensity can be readily tuned by changing the input polarization of the excitation beam. (Chapter 4 will provide more details about this problem from simulations perspective.)

### 3.2.2 Remote excitation SERS

To further probe the antenna effects of the system, the remote excitation properties were decided to be tested, wherein one end of the nanowire is to be excited and the signal is collected from the distal end of the wire. As previously mentioned in the introduction, Ag nanowires on glass substrates have been shown to give propagation of 632.8 nm light and remote excitation SERS in the literature. [20, 44, 79, 80, 81] Thus, remote excitation SERS properties of the modified system are an important set of experiments that would probe the antenna effects of the system further. Such effects are extremely important in nano-communication, as the excitation point is different from the collection point, and information is being transferred from one point to another using a nanoscale waveguide. The system is also great for experiments in the Fourier space as there is a fixed k-vector associated with the light out-coupling at the distal end [20, 81]. Coupling molecular excitation to excitation of particular k-vectors lead to information about extremely important effects which can prove very difficult to probe otherwise. However, the studies in Fourier space are beyond the scope of this thesis and will be studied in greater detail elsewhere.

To study remote excitation effects of the system, a different setup had to be used. The setup is home-built, and is coupled to a Horiba IHR320 imaging spectrometer. A 632.8 nm He-Ne laser was used for excitation, and a 100X 0.95 NA objective lens was used for excitation and detection. The setup is built by Mr. Adarsh Vasista. Figure 3.9 shows the schematic of this setup. As can be seen in the schematic, a notch filter has been used to cut down the Rayleigh scattered light from entering the spectrometer or the CCD. A pin hole has been placed at a conjugate image plane to spatially filter part of the image, so that the spectrometer will only give spectrum of the signal out-coupling from the region that has been selected after spatial filtering. This setup is extremely versatile, and one can place multiple optical elements such as analyzers, beam-splitters, wave-plates, etc. on both the input end and the output end to suit the experimental needs.



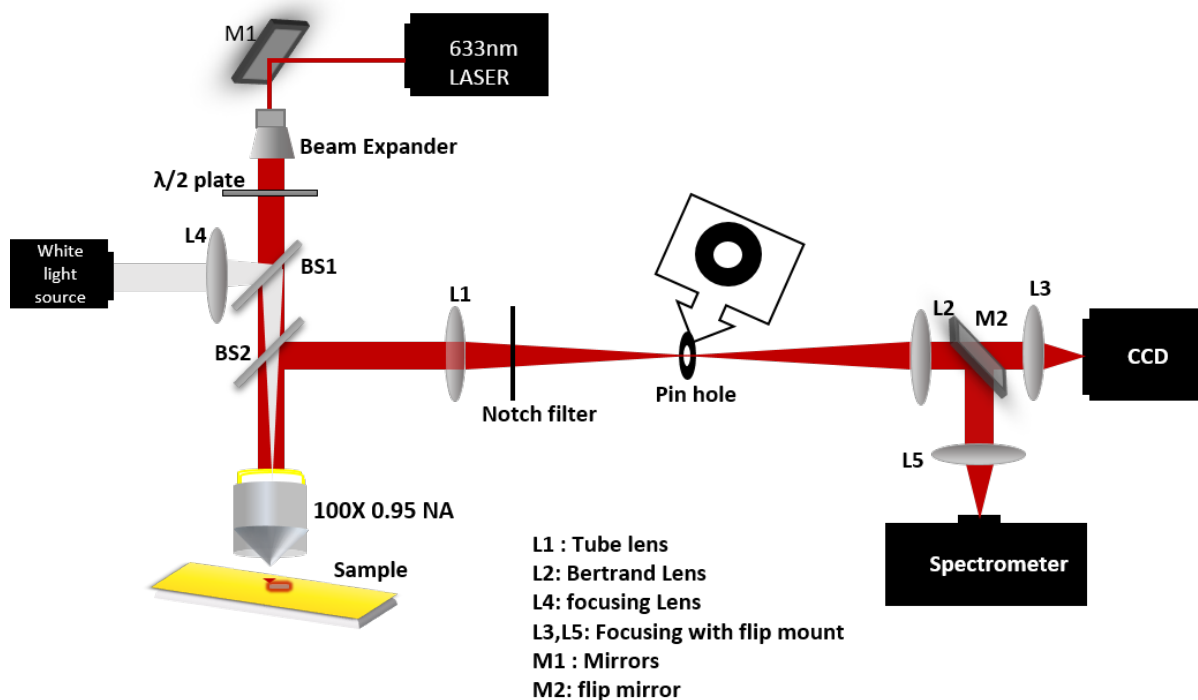


Figure 3.9: Schematic of the setup used for all remote excitation experiments. A 632.8 nm He-Ne laser was used to carry out all the experiments. A  $\lambda/2$  plate was used to rotate the polarization of the input beam. 100X 0.95 NA objective lens was used to focus the laser light onto one end of the wire, and also to collect the signal to be analyzed in the spectrometer. The notch filter was used to filter out the excitation wavelength. Pin hole was placed in a conjugate image plane and was used to spatially filter out the excitation spot and only let through the distal end signals. M2 was used to either visualize the image after spatial filtering in the CCD or to take the spectrum of the signal in the spectrometer.

There were a few changes in sample preparation at this point which need to be noted. Firstly, the gold film thickness was increased to 170 nm to increase reflection and avoid leakage of radiation through the film to the glass side. Secondly, instead of mixing the Ag wires and the dye and drop-casting the mixture onto the film, the following procedure was used:

1. Wash the gold film with acetone and ethanol to clean any impurities from the surface; blow-dry the film.
2. Drop-cast  $10^{-6}$ M Nile Blue solution in ethanol onto the gold film
3. Once the Nile Blue solution dries, wash the film again with ethanol to remove any excess dye molecules which are not in contact with the Au film
4. Drop-cast Ag wire solution onto this film, let it dry.

This procedure makes sure that majority of the molecules are in contact with the film, and hence have their fluorescence quenched, and also ensures that most of them are sandwiched

between the wire and the film, which is exactly where we want them to be. These changes leads to higher signal intensity, which is crucial for such remote excitation experiments.

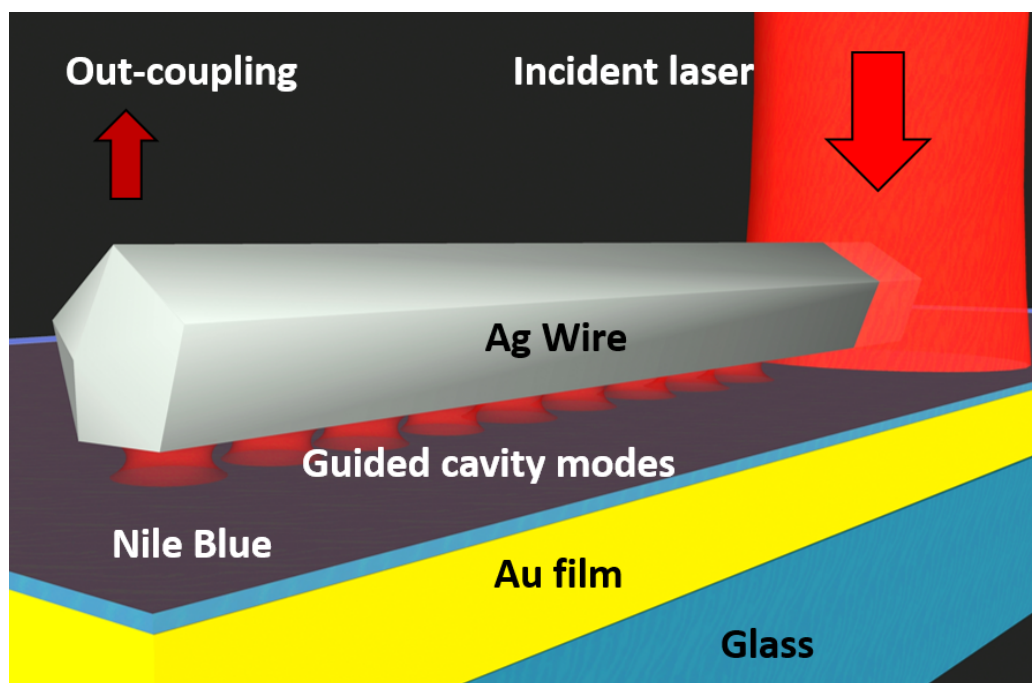


Figure 3.10: Schematic of the system used for remote excitation based measurements. The Au film thickness was increased to  $\sim 170$  nm, and the NB molecules were first drop-casted onto the film, onto which the Ag wires were deposited to ensure that maximum molecules are inside the gap.

Figure 3.10 shows the schematic of the wire film system when one excites one end of the wire and collects at the distal end. Figure 3.11 shows the optical image of the wire under (a) white light illumination and (b) when one end of the wire has been excited. Out-coupling of the 632.8 nm light can be clearly seen at the distal end of the wire. An interesting question to ask is: What signals do we observe at the distal end of the wire, apart from the laser light that is being out-coupled? It is quite possible and expected that the plasmons (both SPP along the wire and the gap plasmon in the cavity) will excite molecules along the wire. This photons from the de-excited molecules can then couple back to the SPP and get out-coupled at the distal end. It is also possible that the 632.8 nm photons that are getting out-coupled at the distal end excite molecules AT the distal end and we can get this signal in the spectrometer. It is also possible that there is some localized component of electric field along the wire (including at the end of the wire) which gives rise to signal.

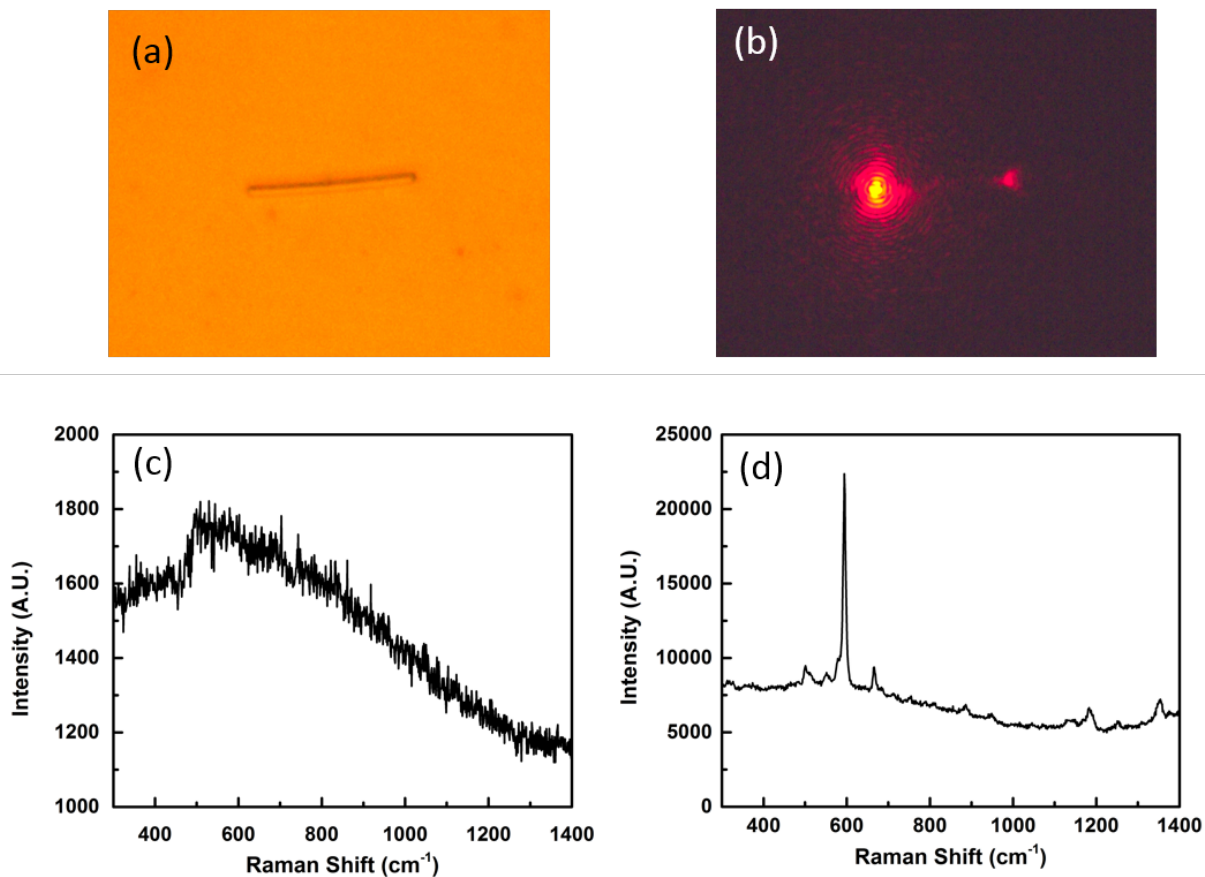


Figure 3.11: Optical image under (a) white light illumination, and (b) when excited by 632.8 nm laser at one end of the wire. The distal end is glowing, indicating that there is propagation through the wire SPP, the gap plasmon or a combination of both. (c) Spectra at the distal end in the absence of gold film under the wires. Weak fluorescence is observed, as there is no film to quench the fluorescence or no cavity to enhance the emission. (d) Clear Raman signal riding over small amount of fluorescence is observed at the distal end in the presence of the gold film, indicating that the interaction between the film and the wire is leading to enhancement of the Raman signal while quenching the fluorescence.

Before probing these effects, it is important to do a control experiment, that is to test what happens at the distal end if we do the same experiment as above, but without the gold film. This knowledge is important as it will give us an insight about the role of the gold film. Figure 3.11(c) shows the signal that was acquired at the distal end of the wire when coupled to a glass film. We clearly see that there is no Raman signal getting out-coupled at the distal end, and only a broad and weak fluorescence peak is visible. This is because the Nile Blue molecules are not in direct contact with any metal, and secondly the signal is being taken at the distal end, by which point there are large propagation losses, thereby reducing the signal intensity.[17]

Figure 3.11(d) shows the spectrum acquired at the distal end of a wire when placed on a Au film. The spectrum shows large Raman intensity at the distal end, with some amount of fluorescence background. The  $590\text{ cm}^{-1}$  line is clearly visible in the spectrum, indicating

that it is indeed the Nile Blue Raman spectrum that is being out-coupled at the distal end. As mentioned before, the mechanism for this cannot be concluded by seeing only this data, and hence a series of experiments need to be done to be able to decipher the exact mechanism of such a signal at the distal end.

The first check that needs to be done is, whether a gap plasmon is really being generated between the wire and the film, and what is its contribution to the signal. One way to ascertain this is simulations, which has been done in Chapter 4. An experimental check would be to test if any signal is observed in the center of the wire, where there is no out-coupling of the photons to excite molecules locally. Figure 3.12 compares the spectrum acquired at the center of a wire with the spectrum acquired at the distal end of the same wire, when the excitation was at one of the ends. As can be clearly seen, there is a large amount of Raman signal even at the center of the wire, albeit smaller in comparison with what is observed at the end of the wire. The difference could possibly be attributed to the out-coupled photons exciting molecules locally at the distal end. However, this ascertains the fact that there is indeed a large intensity of electric field all along the cavity between the wire and the film, which is due to a gap plasmon being generated in the cavity. It can be said that the gap plasmon is a major contributor to the signal because of the huge field confinement that happens in the gap. This will be later discussed in the context of simulations in Chapter 4.

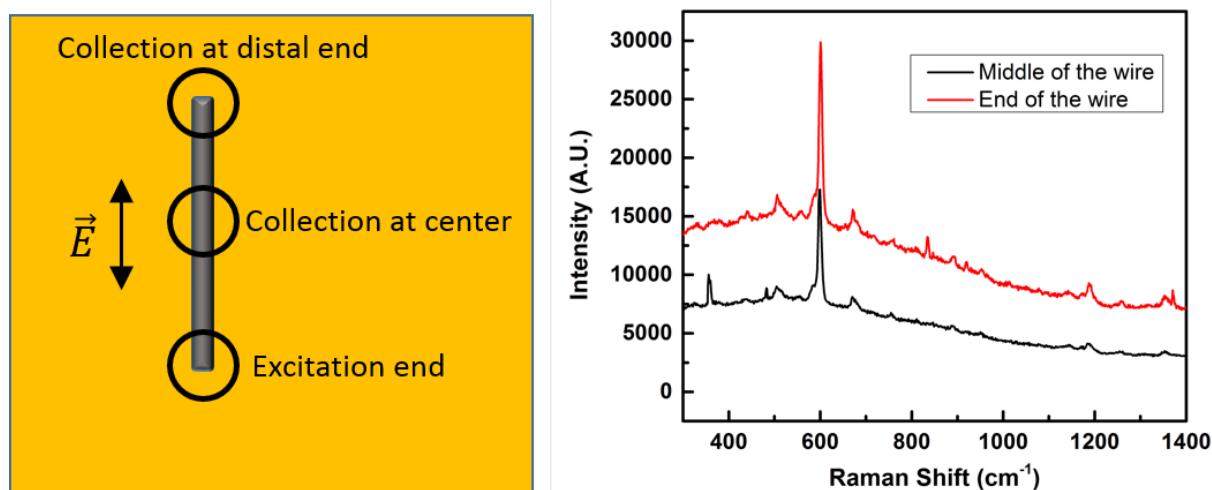


Figure 3.12: (a) Schematic of two collection points of spectra taken in (b). (b) Spectra comparing the emission collected from the distal end of the wire with the emission collected from the center of the wire. Excitation was done at one end of the wire in both cases. The emission from the center is clearly because of the existence of gap plasmon that is exciting the molecules all along the wire. The difference in intensity at the end and center spectra is most likely due to the out-coupling photons at the end exciting the molecules locally, which does not happen at the center.

## Input polarization dependence

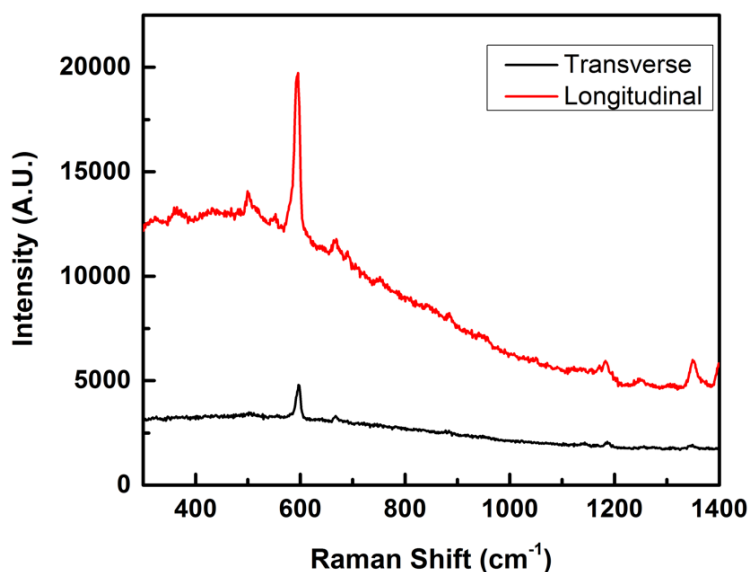


Figure 3.13: Input polarization dependence of the spectra at the distal end of the wire. As expected, the signal is maximum when the input polarization is longitudinal, due to generation of propagating modes along the wire and the gap. However, the observation of Raman signal at the distal even in case of the input field polarization perpendicular to the wire is interesting. The reason for this observation is the gap-plasmon field which propagates even when the input field has transverse polarization.

To further probe the effects of the system on the SERS output at the distal end, input polarization was varied to test the spectrum at the distal end. Input polarization is an important parameter while studying SERS effects, as the Raman cross-section depends on the incident polarization [82] depending on the Raman mode that is being taken into consideration. Input polarization is also an important parameter to probe the plasmonic properties of the system itself. For Ag nanowires kept on glass, it has been shown that the propagating component of the surface plasmon along the wire is not excited if the polarization is perpendicular to the axis of the wire. [17] When the polarization is along the wire, the fundamental  $m = 0$  mode of the SPP is excited, while for polarization perpendicular to the wire the  $m = 1$  mode will be excited [83], where  $m$  is the integer measuring the mode winding [15]. However, since this is a different system due to the presence of the gold film under the Ag wire, input polarization dependence had to be checked. Thus, the signal at the distal end was probed for two input polarizations: along the wire (longitudinal) and perpendicular to the wire (transverse). Figure 3.13 shows the two spectra on the same scale for comparison. It can be seen that the spectra when the input polarization is along the wire is much larger than that when the polarization is perpendicular to the wire. Here, the SERS differential cross-section will not come into picture strongly as the molecules are most likely arranged randomly inside the cavity, and thus any effects of input

polarization on the molecules will be averaged out. But what we observe can be explained by looking at the plasmonic properties of the system. When the input polarization is along the wire, SPP is generated along the wire. This leads to larger electric field intensities along the wire and in the gap, thereby enhancing the emission of the molecules in the cavity. The enhancement is much larger as compared to when the input polarization is perpendicular to the wire and the field is heavily localized at the excitation end. However, what is interesting is that there is still Raman signal observed at  $590\text{ cm}^{-1}$  at the distal end, even though the SPP along the wire has not been excited. This signal is probably due to the gap plasmon, which leads to some amount of electric field along the wire, thereby exciting some molecules in the gap. The field profiles shown in Chapter 4 indicate towards the same. This is an interesting effect that one can see in this hybrid system, which has a non-zero propagating component even if the incident field is perpendicular to the direction of propagation.

### **Output polarization of the signal at the distal end**

In the case of a silver nanowire supported on a  $\text{SiO}_2$  (glass) substrate, the excitation of the  $m = 0$  mode, when it out-couples at the distal end leads to emission which is polarized along the wire, while the out-coupling of the  $m = 1$  mode results in emission polarized perpendicular to the wire.[83] However, since we also have cavity modes and the film SPP mode in the present scenario, the hybridization of these modes will lead to modification in the polarization states of the out-coupling photons. Thus to test the effects of these modifications on the out-coupling photons, the signal at the distal end was analyzed by placing an analyzer in its path with polarization (i) along the wire and (ii) perpendicular to the wire. Figure 3.14(c) shows the resolution of the signal with respect to the output polarization. The input polarization for all the studies was kept parallel to the axis of the wire to maximize the output signal. The figure indicates that the out-coupling signal has a larger intensity with polarization perpendicular to the wire as compared to polarization along the wire. This is counterintuitive, as the SPP along the wire is polarized along the wire, and hence the out-coupling photons should have a larger component along the wire as compared to perpendicular to it. This effect is clearly due to the interaction of the SPP with the cavity modes and the film SPP. To test this hypothesis, FEM simulations were done to find the profiles of the transverse and longitudinal components of the electric field in the gap. Chapter 4 deals in more detail about this issue. To briefly summarize, the conclusion that can be drawn from the simulations is that the field intensity in the gap as well as along the wire perpendicular to the wire is stronger than the field parallel to the axis of the wire. The reason for this effect is still unknown, and further studies are under way to completely understand this effect.

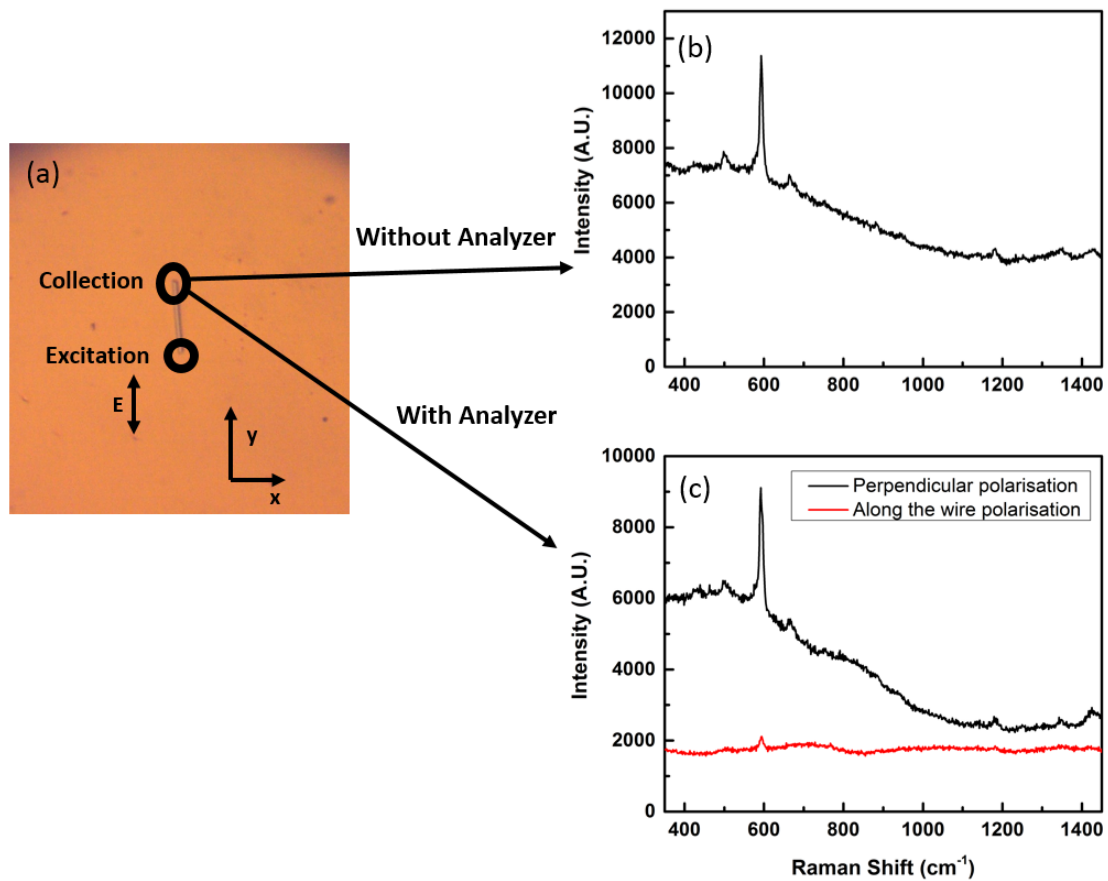


Figure 3.14: (a) Details about the excitation and collection geometry used for output polarization dependent measurements. (b) Spectrum observed at the distal end without any analyzer in the signal path. (c) Spectra observed after using analyzer. The dominant contribution is clearly due to electric field polarized perpendicular to the wire.

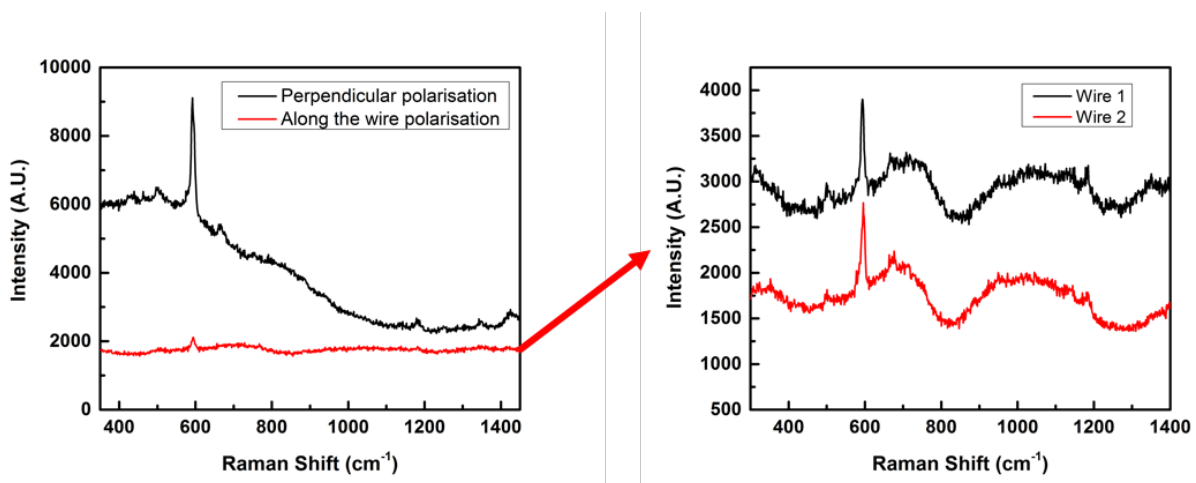


Figure 3.15: Spectrum for output polarization along the wire zoomed in on an appropriate scale. Data has been shown for two different wires of varied lengths and thicknesses. The undulations observed are at the same spectral positions for both the wires.



There is another interesting observation that can be seen in the spectrum with analyzer position along the wire. Figure 3.15 plots the spectrum on a more appropriate scale. This reveals pronounced crests and troughs in the fluorescence background, with a shift of 300-500  $\text{cm}^{-1}$  between successive crests and troughs. What is more interesting is that these crests and troughs are at the same position spectrally for various different wires, with different lengths and thicknesses. The reason for this is hypothesized to be cavity modes with resonances normal to the film. Such modes have been observed in a similar system but under a different configuration, wherein the excitation and the collection points are the same.[59] However, more experiments need to be done to ascertain the exact origin of these undulations.

### **Input power dependence**

Input power dependence of the SERS signal of Nile Blue from the system was observed at both the excitation end and the distal end. This serves two purposes: (i) it helps us identify if there are any non-linear processes that are occurring in the system, and (ii) it helps us identify at what power we get SERS. The lower this threshold, the better it is, as even on putting in small amounts of power, we can extract Raman signals from the system. Figure 3.16 shows the input power dependent spectra at (a) the excitation end and (c) the distal end. (b) and (d) are plots of the 590  $\text{cm}^{-1}$  peak for each value of input power. The input power was measured in  $\mu\text{W}$  and was measured using Coherent LabMax-TOP Laser power and Energy meter. It can be seen in Figure 3.16(a) that SERS signal is observed at the excitation end even for input powers of  $1.61 \pm 0.02 \mu\text{W}$ , which is low power for Raman scattering to be observed. This shows that the plasmonic wire-on-mirror system is capable of enhancing the electric fields to a large extent even with extremely low input powers. The signal saturates after a certain intensity (386  $\mu\text{W}$  as observed here). This is possibly due to photo-bleaching of the molecules, or due to complete dissociation of the Nile Blue molecules. The extremely high electric fields possibly lead to dissociation of the bonds of the Nile Blue molecules in the cavity, which thus reduces the spontaneous emission observed.

At the distal end, the minimum power observed to give SERS signal was  $89 \pm 1 \mu\text{W}$ , but it is possible that SERS signal is observed even for lower values of input power, but simply could not be probed due to lack of resolution in the input power.

Figures 3.16(b) and (d) show that the log-log plots of the peak intensity vs the input power are linear both at the input end and the distal end. The slopes of both the graphs are less than unity, indicating that this is not any form of stimulated emission, which should have a slope greater than 1. Large propagation losses account for the slope reducing from a value of 1 to lesser than 1.



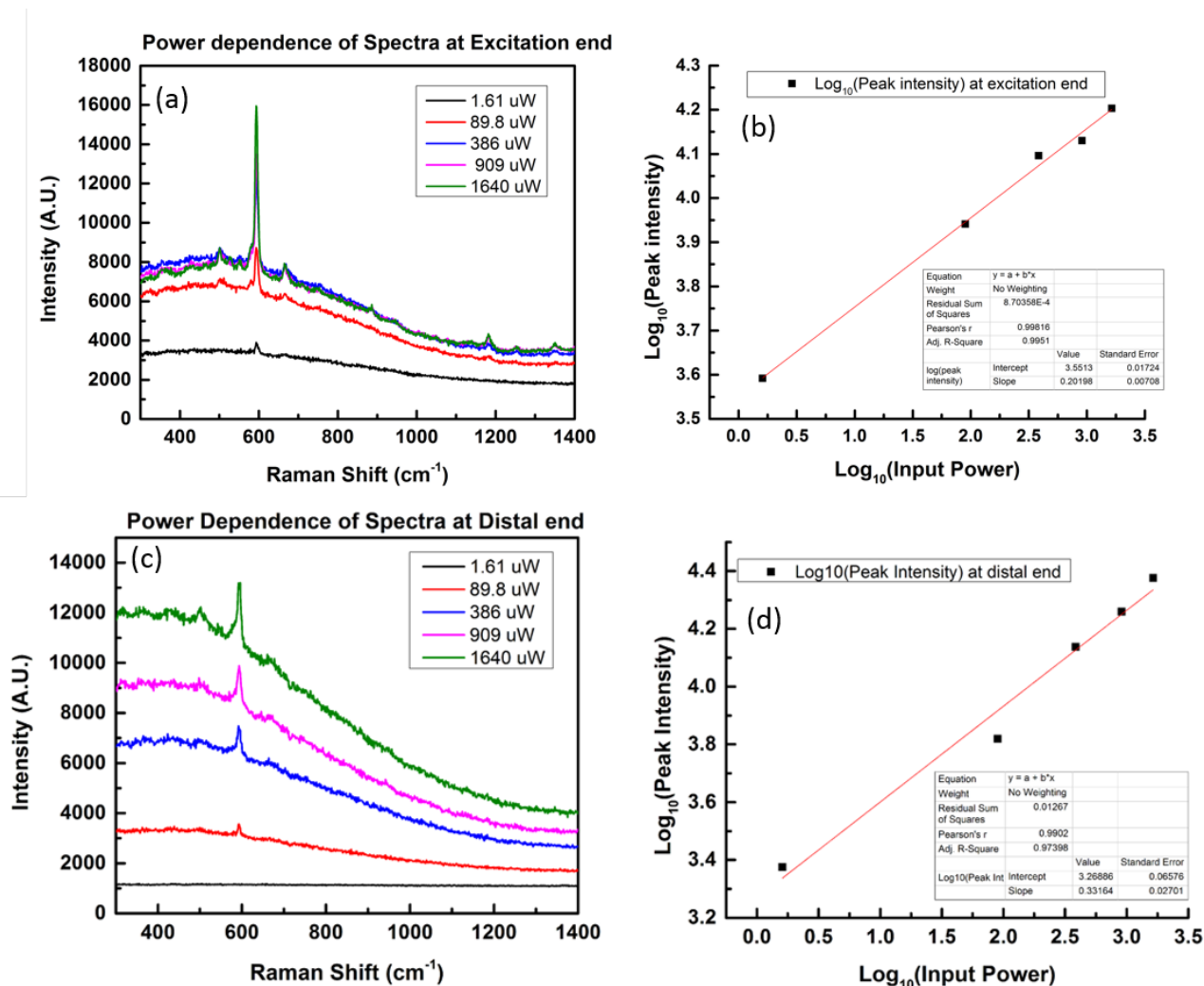


Figure 3.16: (a) Spectra for various input powers acquired at the same end where the wire is being excited. The intensity grows as input power grows up to a certain point, after which it saturates. (b) Log-log plot of the intensity of the 590 cm<sup>-1</sup> line vs the input power. The trend is linear with a slope less than 1, indicating large amount of losses. (c) Spectra for various input powers acquired at the distal end of the wire. The intensity grows till 1.61 μW. (d) The log-log plot of the intensity of the 590 cm<sup>-1</sup> line vs the input power. The trend is linear with a slope less than 1. This is also due to large propagation losses in the wire and through the cavity.

### Effects of spacer layer between molecule and gold film

Finally, to probe what happens if the molecules are not in direct contact with the bare gold film, but some distance away from it. This is an important experiment as it gives the information about the interaction of the metal film with the Nile Blue molecules, and helps in probing the cavity system in greater detail.

To carry out this experiment, a gold film of thickness  $\sim 170$  nm was coated with a thin layer of SiO<sub>2</sub> ( $\sim 10$ nm) by sputtering method. SiO<sub>2</sub> is a dielectric, and so it was coated on the gold film to act as a spacer layer. Nile Blue ( $10^{-6}$  M) was deposited on top of the SiO<sub>2</sub> layer, dried,

and once washed with ethanol. This ensured that the Nile Blue molecules were not in direct contact from the gold film, but were not extremely far away either, leading to their fluorescence being enhanced instead of being quenched. Silver nanowires were drop-casted onto the Nile Blue film. One end of the Ag wire was excited using 632.8 nm laser, while the spectrum at the distal end was captured in the spectrometer using spatial filtering. Figure 3.17(a) gives a schematic of the modified system, while (b) gives the spectrum observed at the distal end of the wire. Clearly, there is no  $590\text{ cm}^{-1}$  Raman line observed in the Nile Blue spectrum. Only fluorescence is seen, which has been enhanced due to the presence of the metal wire and the metal film in the vicinity of the molecules. Fabry-Perot modes are also seen riding on top of the fluorescence profile, which are due to the cavity between the wire and the gold film including the  $\text{SiO}_2$  layer. This clearly demonstrates the role of bare gold film in contact with the Nile Blue molecules, which is to quench the fluorescence of the molecules, after which the enhanced electric field in the cavity can enhance the Raman intensity of the Nile Blue molecules.

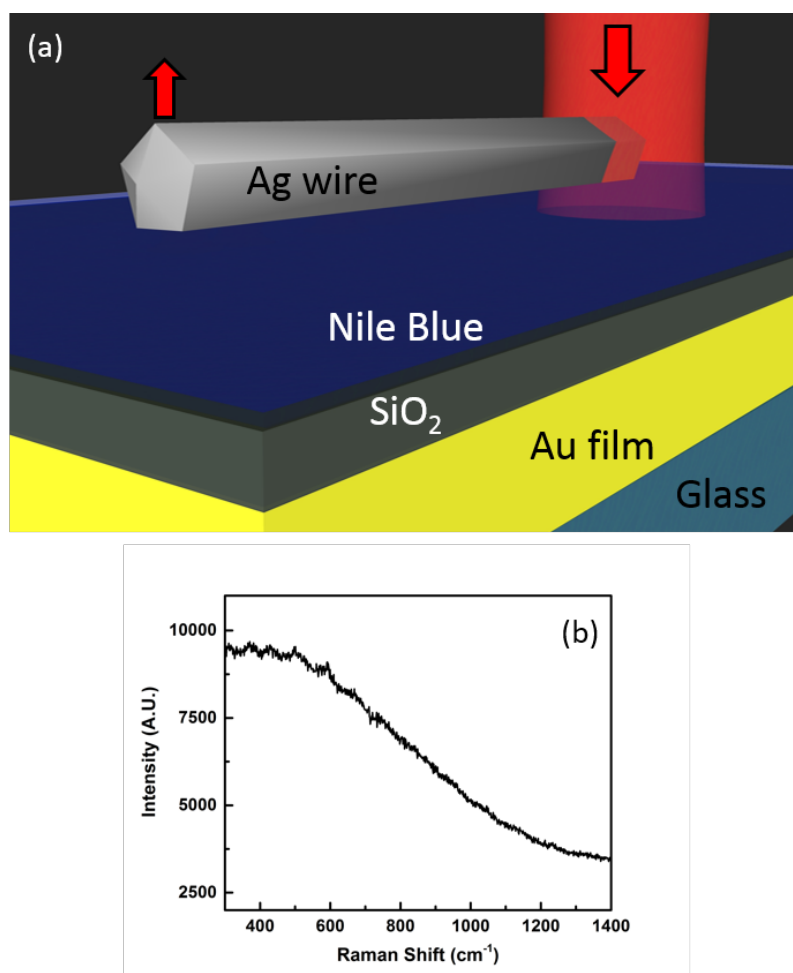


Figure 3.17: (a) Schematic of the modified system with  $\sim 10\text{ nm}$   $\text{SiO}_2$  layer on a  $170\text{ nm}$  gold film. Nile Blue ( $10^{-6}\text{M}$ ) was drop-casted onto the  $\text{SiO}_2$  layer, followed by drop-casting of Ag nanowires. (b) Spectrum as observed at the distal end of the wire. Pure fluorescence was observed, with Fabry-Perot modes riding on the spectrum.

### 3.2.3 Conclusions for Chapter 3

This chapter has thus tried to tackle two different systems: (i) gold nanorods on gold film with Nile Blue, and (ii) silver nanowires on gold film with Nile Blue. For the gold nanorods-on-film system, enhancement of the Nile Blue Raman signal has been observed for various particles. The polarization dependence of the Nile Blue was attempted to be studied in this system, but correlation with SEM imaging is required to conclusively prove the polarization dependence of the signal. For the silver-wire-on-mirror system, enhancement of the Raman signal was observed. The signal showed a  $\cos^2\theta$  behavior as a function of input polarization, which was corroborated with numerical simulations. Remote excitation SERS was observed, which showed dependence on input power and input polarization. The output polarization studies gave some insight about the mechanism of out-coupling at the distal end, which is that the dominant component of the out-coupling photons is due to the electric field component (along the wire and in the gap) that is perpendicular to the direction of propagation. This counter-intuitive effect warrants some further investigation, which is currently being done. Finally, the effect of the bare gold film was checked by sputtering  $\text{SiO}_2$  spacer layer of  $\sim 10$  nm and carrying out the same experiment. It was observed that no Raman signal is observed, and there is large amount of fluorescence, indicating that the bare gold film, as previously hypothesized, was quenching the fluorescence and thereby leading to enhanced Raman signals from the Nile Blue molecules.

# Chapter 4

## Simulation studies of Ag wire on Au film system

Giving theoretical backing to a set of complicated experimental details is a good and necessary practice. Firstly, it confirms that the experiments are correct, and the method of reaching the inference from the conclusions is logically consistent. It is necessary to have such confirmation, especially in cases where the experimental setup is extremely complex. Secondly, if the experiment doesn't match with the theory, then there is a problem with either the way the experiment was done, or the theory is somehow lacking, and that leads to progress in the field. Such theoretical backing, at least in case of nano-optics, is usually obtained by solving a set of boundary-value problems to known ordinary or partial differential equations for the system under consideration.

However, analytical solutions are usually available only in cases of "easy" geometries with high degree of symmetry, uncomplicated materials, and "well-behaved" boundaries. Such solutions are extremely difficult to find when the systems under consideration are complicated, with reduced symmetries and materials with complex behaviors. In such cases, the differential equations are either simply not solvable by analytical means, or are extremely complex and require high amount of computational power. It is then easier to resort to numerical means to find approximate solutions to the problems. These solutions have to be physically acceptable, and have to be as close to the real scenario as possible. There are multiple methods of finding such approximate solutions, including Finite Element Method (FEM), Finite-Difference Time-Domain method (FDTD) and Surface integral method.

For the purpose of finding approximate solutions to the problems addressed experimentally in this thesis, Finite element method was chosen for the computational analysis. COMSOL Multiphysics<sup>®</sup> is a commercially available software which employs this method to solve problems numerically. Briefly, the formulation in the Finite element method is to convert the system of ordinary differential equations into a system of algebraic equations.[84] The system for which the solutions are to be obtained is divided into smaller parts, called finite elements, and

this process is called discretization or meshing. The solver then solves the set of equations for each small part separately, and in the end puts all the solutions together in a way that complies with a set of continuity conditions for each "node" (common point between two neighboring elements) or boundary lines/surfaces. The end result is that we get the solution of the problem at discrete points of the body, the resolution of which depends on the computational resources at hand. Thus to get more accurate results, more computational power has to be invested. To conclude, FEM solves the problem at a set of discrete points and then combines all of it to give us an approximate solution for the problem at hand.

As mentioned previously, simulations give theoretical backing to the experimental results, as well as give new insights to the system used. Both of these has been attempted here by using numerical simulations for the system of Ag nanowire on gold film system. The solutions are limited by the computational resources available, but are fairly accurate as they have been matched with results known in literature at more than one occasions. Thus, the method is reliable and the results given below can be considered to model the real system.

## 4.1 Basic parameter details

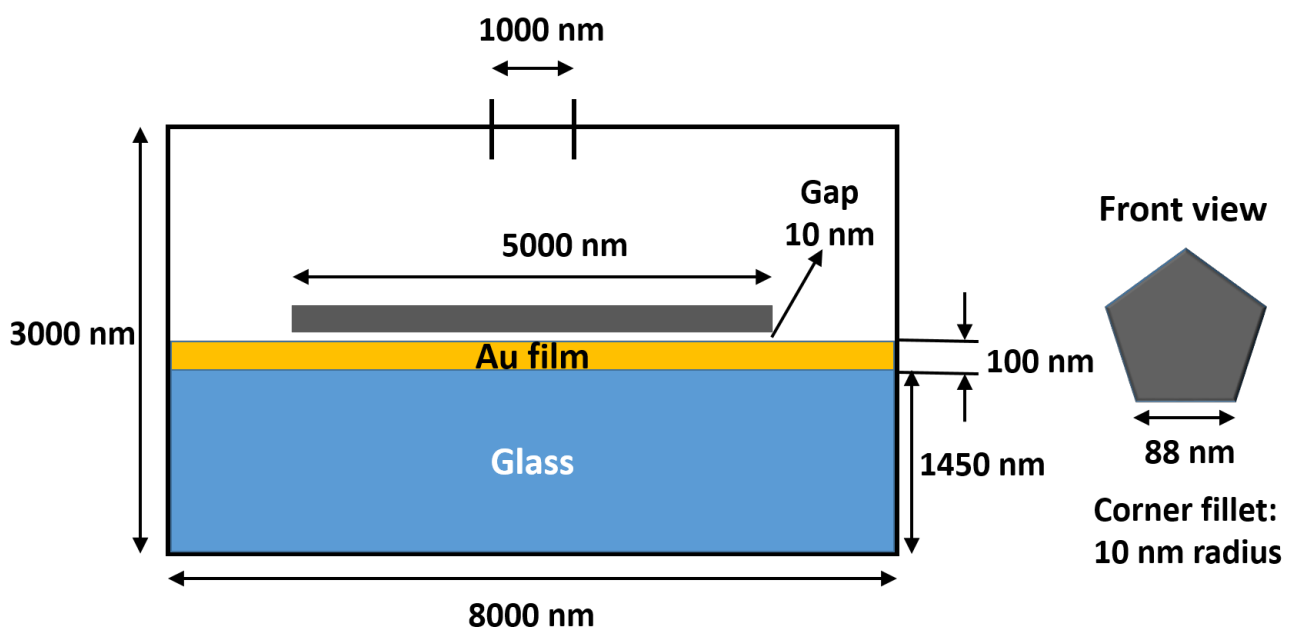


Figure 4.1: The parameters used for simulations in this chapter. The parameters were optimized in order to closely resemble the real situation but also to keep the simulation memory requirements within the constraints available.

Before doing the actual simulations, one has to optimize the size of the simulated objects and the meshing parameters so that convergence is achieved in the least possible iterations, and

physically realistic solutions are obtained. The memory of the computer being used is also a constraint to be considered, as the simulation will stop working if the computer RAM is exceeded in the course of the simulation. Keeping these constraints in mind, the simulations for this chapter were designed. Figure 4.1 details the various dimensions used for the simulations. As mentioned previously, the model has to now be broken up into smaller parts, or finite elements, which will be used to solve the differential equations of the problem. To do so, one has to again keep in mind the balance between accuracy of the result obtained and the physical memory of the computer in used. Thus, the meshing parameters that were used after optimization were as follows:

1. **Air:** largest - 200 nm, smallest - 25 nm
2. **Wire:**
  - Domain: largest - 10 nm, smallest - 5 nm
  - Boundaries: largest - 3 nm, smallest - 2 nm
  - Edges: largest - 3 nm, smallest - 1.5 nm
3. **Film:** largest - 10 nm, smallest - 1.6 nm
4. **Glass:** largest - 150 nm, smallest - 18 nm

As for the materials used for the simulations, the wire was made of Silver (refractive index data given by Johnson and Christy [85]), the gold film was made of Gold (Johnson and Christy [85]) and the glass was made of quartz (with  $n = 1.5$ ,  $k = 0$ ). The excitation was done through the port at the top, and since plane wave excitation was used, the spot size was  $1\mu\text{m}$  to match with the experimental spot size of the laser. The simulations were done at 657.34 nm for the SERS polarization dependence measurements, and at 632.8 nm for the other simulations.

## 4.2 Input polarization dependence for center excitation

The input polarization dependent simulations gave us an insight about the SERS polarization dependence, as previously seen in Chapter3 (Figure 3.8). The  $\cos^2\theta$  dependence of the SERS signal follows the  $\cos^2\theta$  dependence of the  $|E/E_0|^2$  of the incoming electric field, which has also been observed in literature in some other context [41]. There is a phase shift in both the field dependence and the SERS enhancement of  $90^\circ$ , as the highest field localization occurs when the incident field is perpendicular to the wire. However, the trend is still  $\cos^2\theta$ , and thus, simulations have been successful in giving us knowledge about the underlying mechanism of the input polarization dependence of the SERS signal observed.

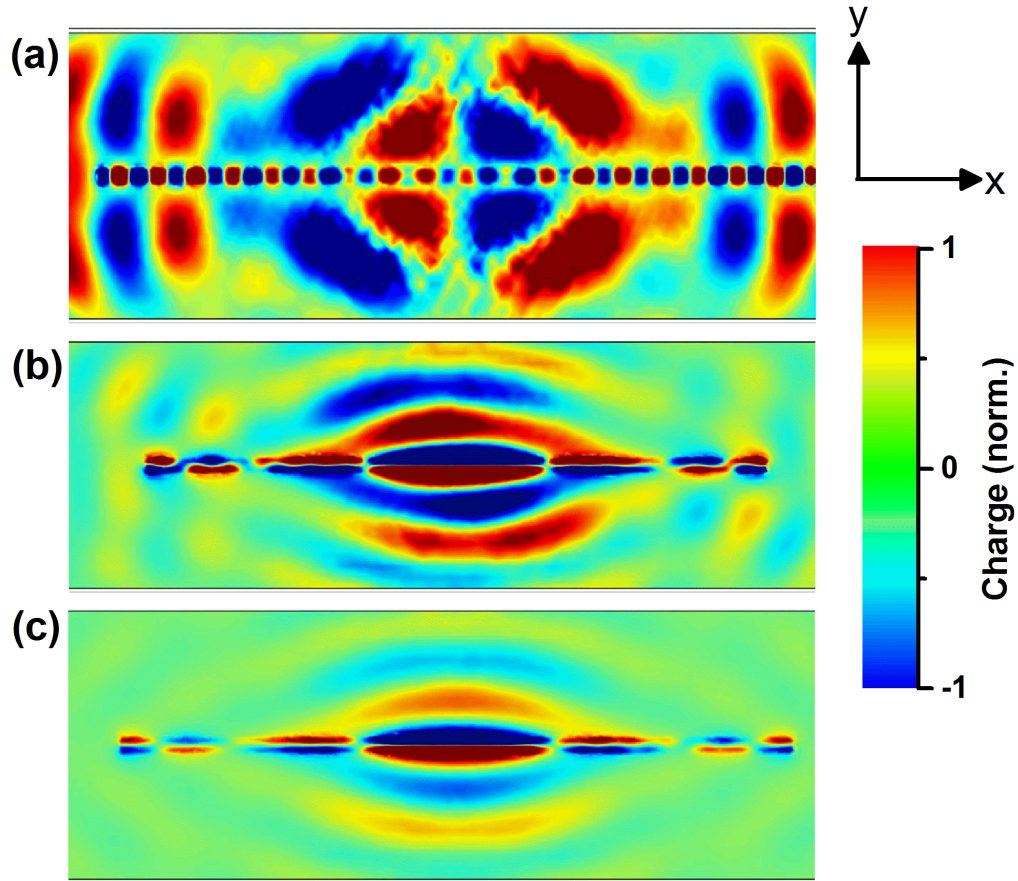


Figure 4.2: The charge distribution on the gold film when the wire is excited at the center with input polarization (a) along the wire, (b) at  $45^\circ$  to the wire axis, and (c) perpendicular to the wire. The wire axis is along the x axis. (a) A clear SPP type mode is observed along the wire with alternate positively and negatively charged regions. An SPP mode is also observed on the film. (b) Chiral plasmon type behavior is observed, possibly due to generation of both  $m = 0$  type mode and  $m = 1$  type mode in the wire. (c) Very weak propagation is observed along the wire. The field is highly localized near the excitation region, thereby leading to extremely high SERS signals in this configuration.

However, this is not the only information that these simulations can give. Since the simulations match with the experimental results, we can now extend the scope of these simulations and extract new information from them which cannot be experimentally obtained (at least in the current scenario). For this, the charge distribution on the gold film was calculated using Gauss's law. Figure 4.2 shows the charge distribution on the gold film-air interface for 3 values of polarization. The wire is in the center of each image along the X axis. For the case when the input polarization is along the wire (part (a)) or  $0^\circ$ , one sees clear signs of SPP mode being generated along the X axis. The alternate negative and positive charges are an indicator of an SPP type mode being generated at those points. This is most likely the gap plasmon which is propagating along the cavity. There is also signatures of propagating mode being generated on

the gold-air surface on either side of the wire.

When the input polarization is perpendicular to the wire (part (c)) or  $90^\circ$ , the field is highly localized at the excitation location. There is very weak field along the direction of the wire, and no sign of an SPP like mode is observed along the wire. This leads to large field intensity at the location of excitation, and thus we have the maximum SERS signal coming from the system in this configuration.

An important and interesting new information that we can see from this exercise is when the polarization is at  $45^\circ$  to the wire axis (part (b)). The charge distribution observed here indicated towards chiral plasmon generation. A chiral plasmon is a plasmon that has an angular momentum associated with it. Structures which show such kind of plasmonic behavior also show circular dichroism, which can be seen by using circularly polarized light onto the wire. Silver nanowires have been shown to display circular dichroism in a different configuration.[86] One hypothesis as to why such behavior is observed in the current configuration is: when the input polarization is along the wire, an  $m = 0$  type mode is being generated in the system, while for input polarization perpendicular to the wire, an  $m = 1$  type mode is being generated. These two modes have a phase shift of  $90^\circ$ . Now if the incident polarization is  $45^\circ$ , both  $m = 0$  and  $m = 1$  modes will be generated, which on interference, will have give a plasmon which is circularly polarized, due to the phase shift between the two modes. This is an extremely interesting phenomenon, and should be tested out further using experiments.

This observation also prompted some further questions, which are addressed in the following subsection.

### 4.2.1 Leakage Radiation of chiral plasmons

The generation of chiral plasmon has been studied in various contexts such as metamaterials and arrangements of metal nanoparticles, mainly in the context of enhancing and detecting specific enantiomers of optically active dyes.[86, 87, 88, 89] However, the Fourier space imaging of this phenomenon has not been done, and thus this is an important problem that should be solved. To do this, it was proposed that the wire will be excited at the center and the leakage on the glass slide of the film will be observed in the Fourier space. To see whether such leakage will be observed, a thinner film (50 nm) was used for the simulations. Figure 4.3(a) gives the image of the field as observed from the side. It can be clearly seen that there is leakage radiation that is going through the glass side. Thus, this question can be surely addressed experimentally to probe the Fourier space dependence of the chiral plasmon generated in this system (Figure 4.3 (b)).



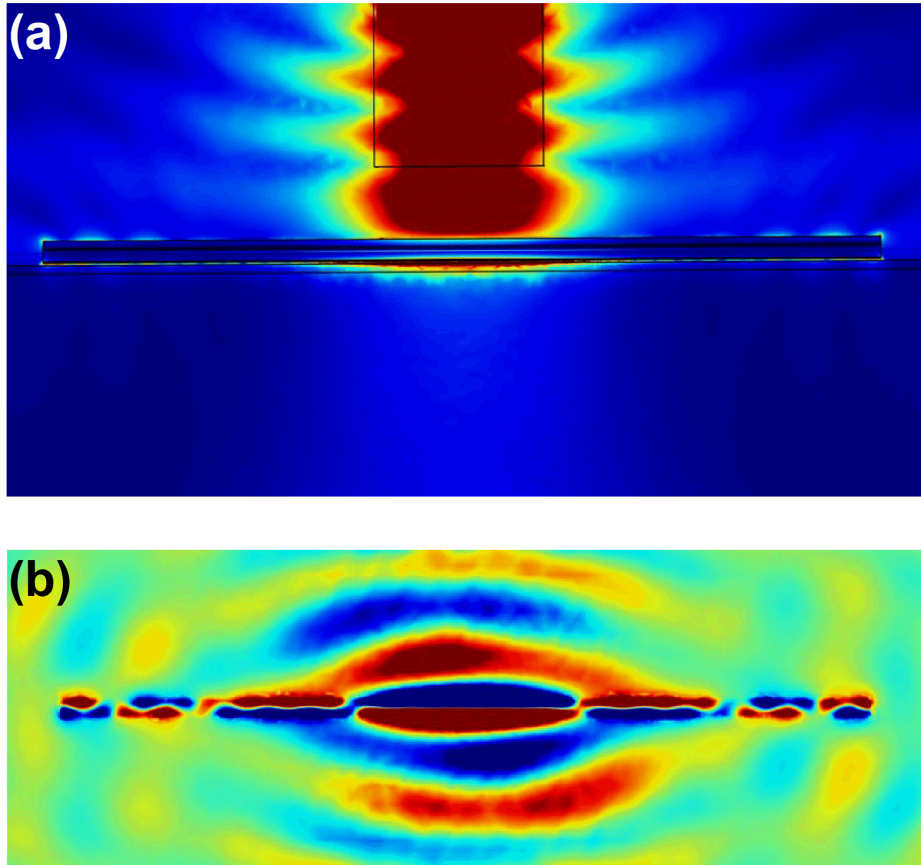


Figure 4.3: (a) Side view of simulations looking for leakage radiation towards the glass side, with input polarization at  $45^{\circ}$  to the wire axis. There is clear plasmon generation at the Au film-glass interface, as well as leakage radiation in the glass substrate. This can perhaps be further studied in more detail experimentally. (b) The charge distribution on the gold film surface (air side). Clear signs of chiral plasmon behavior are observed.

### 4.3 End fire configuration

For understanding the physical phenomena in the end-fire configuration, the input port in the simulations was moved to one end of the wire. The simulations revealed that such excitation leads to generation of SPP along the wire, and also generation of guided cavity modes in the gap. This is true only for excitation with polarization along the wire, while for excitation which is perpendicular to the wire, we see no propagation at the other end of the wire. Figure 4.4 shows the plasmonic landscape for 3 different input polarizations. As can be seen, for an input wavelength of 632.8 nm, the SPP for both the  $0^{\circ}$  case (Fig.4.4(a)) and  $45^{\circ}$  case (Fig.4.4(b)), the wavelengths of the generated SPPs are  $\sim 300$  nm, while that of the gap plasmons are  $\sim 125$ nm. This is close to  $\lambda/2$  for the SPP wavelength, and  $\lambda/3$  for the gap plasmon wavelength. One argument for this reduction in wavelength is possibly the change in the effective refractive index

of the modes that are propagating the SPP. However, further analysis is required for concluding that this is indeed the reason.

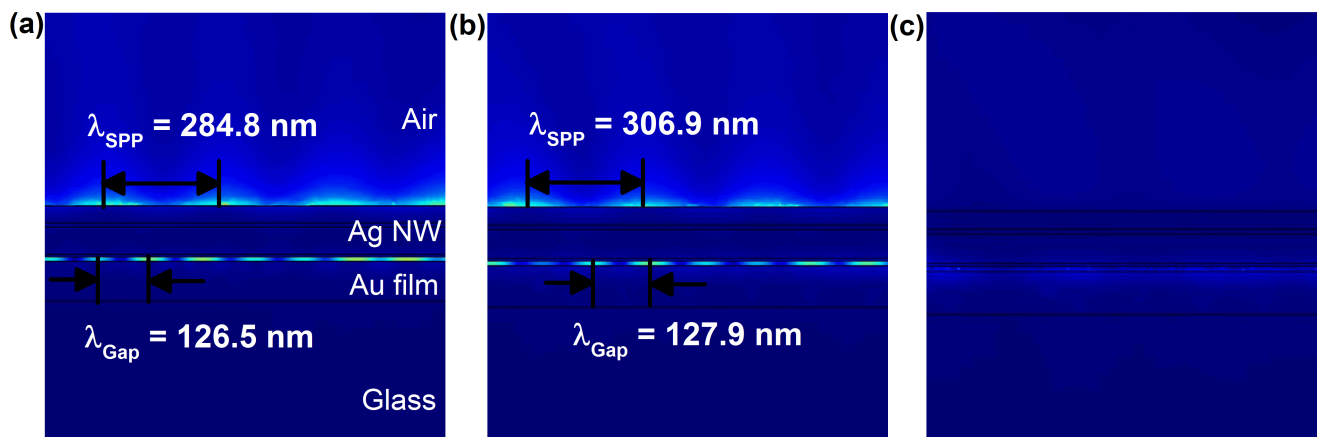


Figure 4.4: Field profiles for section of the nanowire excited at one end with 632.8 nm plane waves with polarization (a) along the wire, (b) at  $45^\circ$  to the wire axis, and (c) perpendicular to the wire. The profiles indicate plasmon propagation along the wire in case of (a) and (b) but not in case of (c). The SPP wavelength along the top edge of the wire in case of polarization along the wire is  $\sim 285 \text{ nm}$ , while the wavelength of the gap plasmon is  $\sim 126 \text{ nm}$ . The SPP wavelength along the top edge of the wire in case of polarization at  $45^\circ$  to the wire axis is  $\sim 307 \text{ nm}$ , while the wavelength of the gap plasmon is  $\sim 128 \text{ nm}$ .

### 4.3.1 Polarization: Input angle dependence

To gain insight about the input polarization dependence in the end-fire geometry, the polarization was varied from  $0^\circ$  to  $45^\circ$  to  $90^\circ$ , to test what phenomena we observe. Fig.4.4 has already given some information about this geometry. Figure 4.5 shows the top view for the three values of input polarization. As can be seen, for  $0^\circ$  input polarization, there is a larger field profile along the wire as compared to the  $90^\circ$  input polarization. There is also a stronger SPP on the film as compared to the  $90^\circ$  case.

For the case of  $45^\circ$  incident polarization, there is chiral plasmon generation in the wire. This phenomenon has been observed experimentally in literature [86]. In Ref.[86], the authors use the chiral plasmon generated using this method to remotely excite a chiral dye molecule and observe remote excitation SERS at the distal end of the wire.

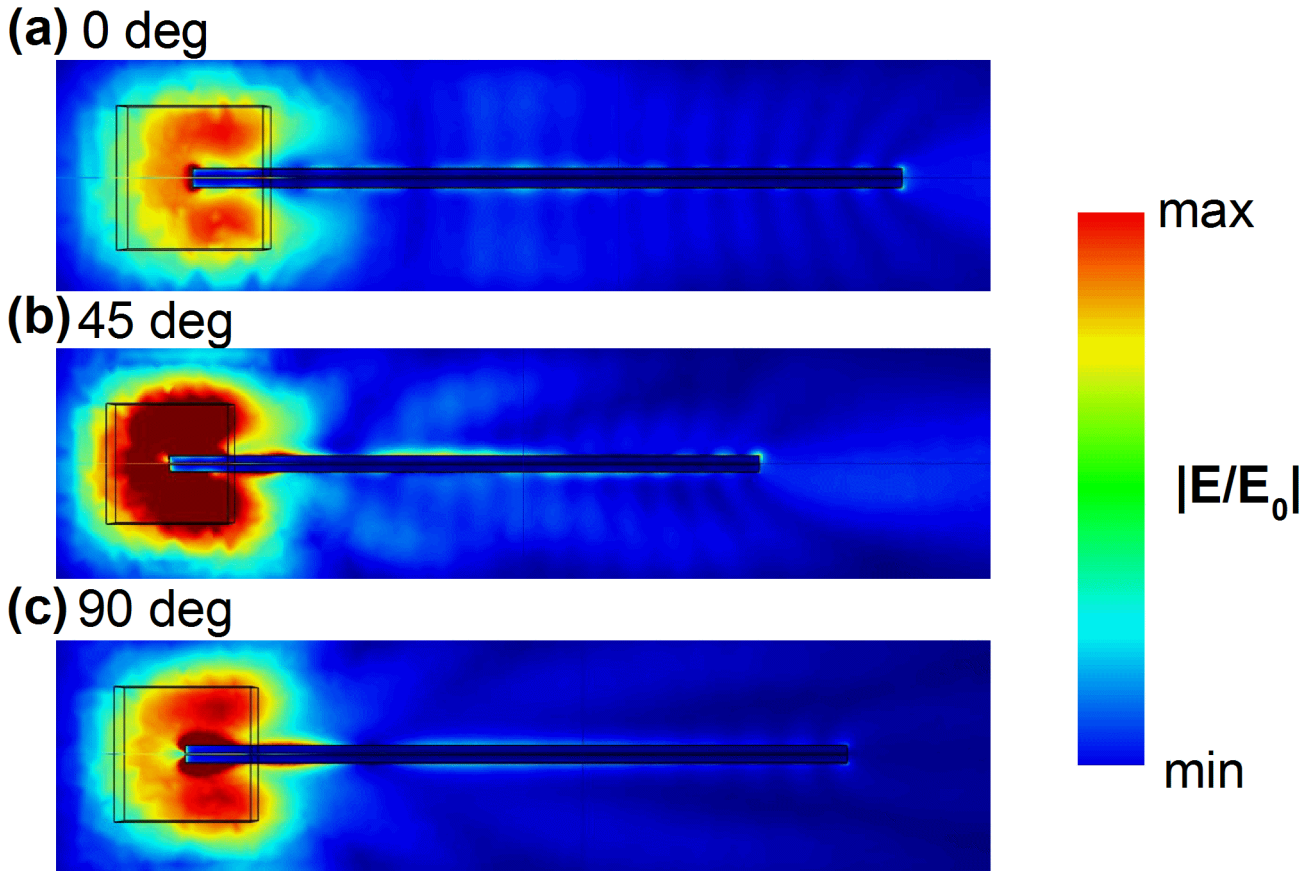


Figure 4.5: Top view of end-fire configuration for three values of input polarization. (a) Propagating plasmon is observed along the film. (b) A chiral plasmon is generated along the film, as observed experimentally in Ref.[86]. (c) No propagating plasmon is observed on the film. The length of the wire in the three images is the same, scale is varying

The cross sectional field profiles for the  $0^\circ$  and  $90^\circ$  input polarization angles are shown in Figure 4.6. Interestingly, the field profiles are different, and for the two values of input polarization, clearly different modes of the wire are being excited. In the case of  $0^\circ$  polarization, all corner modes are being excited, with the top corner mode being strong. The gap has almost uniform field throughout. In the case of  $90^\circ$  input polarization, the top corner mode is not excited at all, while the two bottom corner modes are fully excited. The field is not uniform in the gaps, with more field concentrated near the corners of the wire. This indicates towards fundamental difference in the excitation mechanism of the wire for the two polarizations. To fully understand the exact behavior of the wires under different values of input polarization, one needs to do an eigen-mode analysis of the system, wherein one can find out the different eigen-modes of the wire under various conditions such as input polarization angle. These modes, in this case, will be some form of hybrid modes of the wire, the cavity, and the film. Once

the eigen-modes are identified, the modes observed in experimental scenarios can be given as a linear combination of these modes, and thus one can find the exact mechanism of how a particular mode is being generated. A similar study with a free-standing wire and a wire kept on a dielectric substrate (glass) has been done in Refs.[48] and [24]. However, this study could not be emulated for the system chosen here due to unavailability of eigen-mode solver softwares. Such a study is, however, extremely crucial to further our understanding of this system, as this information will give a deeper insight about the plasmonic interaction that is happening in the hybrid wire-cavity-film system.

It must be noted that the field intensity in the case of input polarization perpendicular to the wire is more than three times that when the input polarization is along the wire. Thus, in case extremely high field confinement is required, one can excite the wire perpendicular to its axis and collect the signal from the same point. This could be especially effective in case one wishes to do single molecule SERS experiments in this configuration.

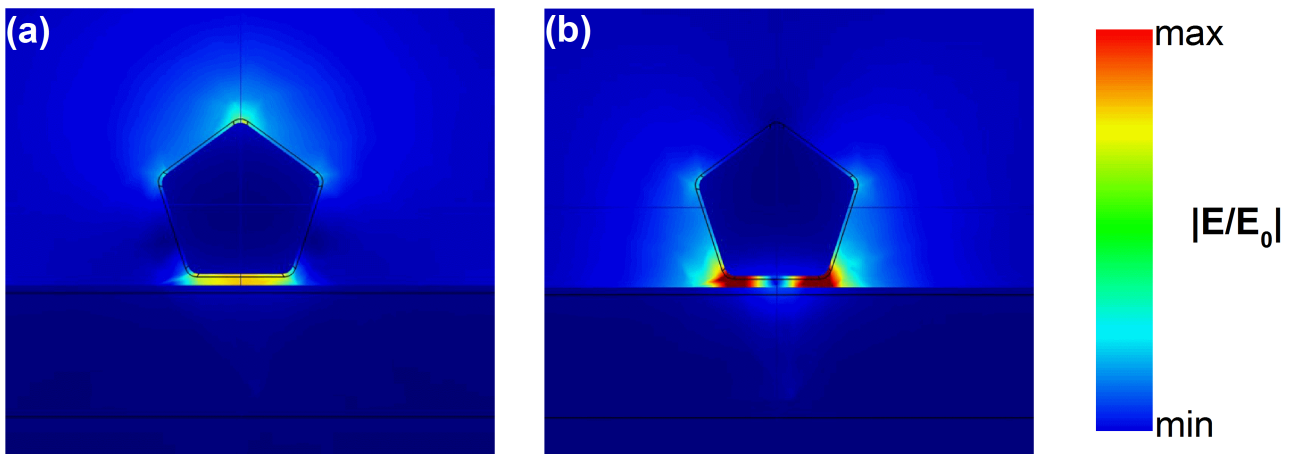


Figure 4.6: Cross sectional field profiles for input polarization (a) along the wire, and (b) perpendicular to the wire. Different corner modes are excited in both cases with different intensities, indicating difference in generation mechanism. The gap plasmon profile is also different in both cases.

### 4.3.2 Polarization: Output angle dependence

An interesting observation, as mentioned in Chapter3 is the output polarization dependence. As mentioned before, the result in this case is counter-intuitive, as the outcoupled light should have a higher number of photons polarized along the wire instead of perpendicular to the wire, but the observation says otherwise. To test this out, the field in the gap of the wire for input polarization along the wire was split into its three components  $E_x$ ,  $E_y$  and  $E_z$ , where  $\mathbf{x}$  is the direction of propagation,  $\mathbf{y}$  is perpendicular to the wire and parallel to the film, and  $\mathbf{z}$  is normal to the film.

The components  $E_x$  and  $E_y$  and their relative strengths are of interest to us. Figure 4.7 shows the field profiles in the gap as seen from the top, while Figure 4.8 shows the fields along the 3 edges of the wire (top, middle and bottom; the profiles for the two symmetric corners will be the same). As can be seen, both the figures show that the fields polarized perpendicular to the wire, or  $E_y$  is much stronger as compared to  $E_x$  all along the wire, except at the distal end of the wire. This implies that the  $E_y$  component must be exciting more molecules as compared to the  $E_x$  component, thereby giving more intensity in the spectrum for this polarization. Thus the simulation gives us some indication as to why there is such difference in the intensities of the two spectra for different output polarization states. This does not, however, explain the undulations in the spectrum for the  $0^0$  output polarization, which needs to be studied in greater detail.

One point to be noted here is that the large meshing in the gap has led to loss of resolution in the field profiles. In Fig. 4.7, there needs to be better meshing in the gap in order to get a more accurate picture of the phenomena happening in the gap of the wire. However, the limited computational power available during the simulations have put a constraint on the meshing, and if possible, these simulations need to be repeated with a smaller mesh in the gap to get a more accurate result for the system.

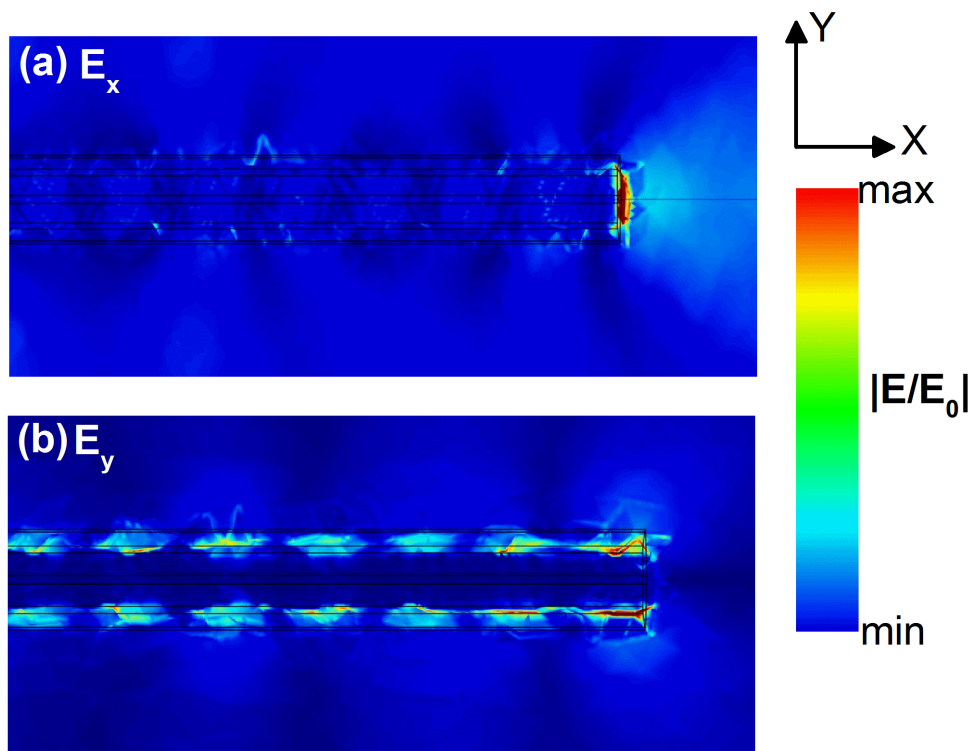


Figure 4.7: Field profiles in the gap between the wire and the film for (a)  $E_x$  and (b)  $E_y$ . The field polarized perpendicular to the wire ( $E_y$ ) is stronger as compared to the field polarized along the wire ( $E_x$ ), which gives a possible explanation for the difference in intensities for the two output polarizations, as seen in Figure3.14.



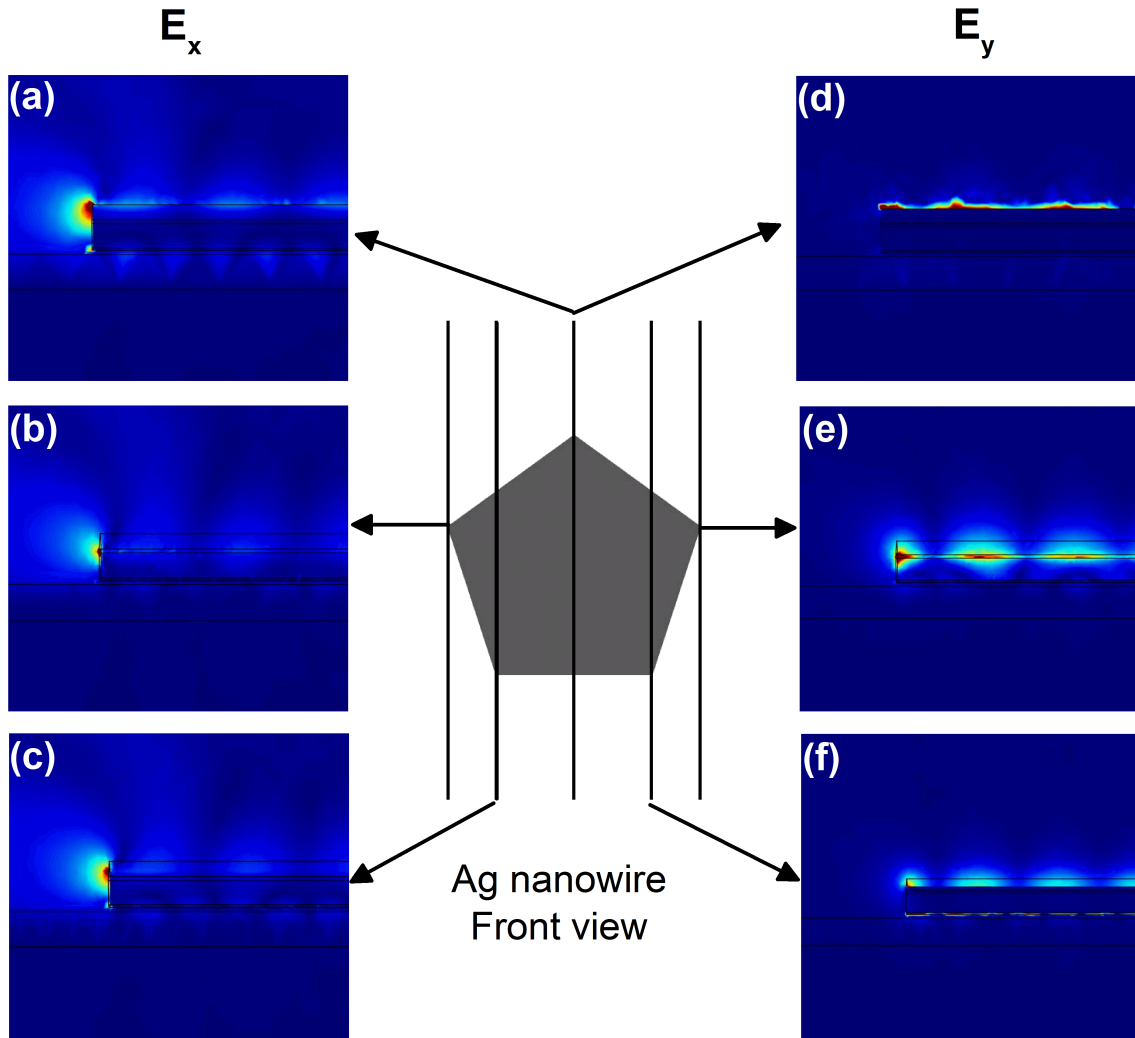


Figure 4.8: Field profiles along 3 corners for the components  $E_x$  ((a)-(c)) and  $E_y$  ((d)-(f)). These profiles also show stronger field intensities for the  $E_y$  component as compared to the  $E_x$  component.

## Concluding remarks

As seen in this chapter, simulations are a great tool, for corroborating results with the underlying theory, giving new insights about the fundamental physics, as well as to find out possible new phenomena which can be tested out with experiments. Better and better simulation methods and tools need to be developed for faster and more accurate simulations, with lesser requirements of computational resources. All the simulations of this chapter can be repeated with a better meshing size in order to gain more accurate results. Other kinds of simulation methods, such as eigen-mode solvers can be incorporated to gain deeper understanding of the phenomena involved in this extremely complex and interesting system.

# Chapter 5

## Conclusions and Future Outlook

Anisotropic nanostructures are, as has been mentioned before, extremely important and interesting especially in the context of nano-optics. The antenna properties shown by such structures need to be studied not only for the applications that they bring forth, but because they reveal a lot about the underlying physics of the process.

Two anisotropic structures, and their interaction with plasmonic film, were studied for the purpose of this thesis. Gold nanorods were synthesized using wet synthesis procedure reported in literature and the Raman antenna effects of the combined rod-gold film system were studied by using the 632.8 nm resonant dye Nile Blue. The Raman enhancement was shown to be extremely high. Some kind of polarization dependence was observed for the signal, but due to technical difficulties, a correlative study was not possible, which would have conclusively determined the Raman antenna effects of single gold nanorods. Nevertheless, this gives an indication for future work as to what difficulties may arise and how they can be solved.

The interaction of a 1D metallic waveguide (Ag nanowire) over a plasmonic film was also studied in context of the Raman antenna effects. The Raman enhancement of this coupled system was shown to be large. The polarization dependence of single Ag nanowire over a gold film was successfully extracted and corroborated with numerical simulations using FEM. Moreover, it was shown that exciting one end of the nanowire also gives huge Raman signal at the distal end, making this an extremely interesting system due to its remote excitation effects. The input polarization dependence was tested out, which showed that even though the wire only propagates light when the polarization is along the wire, the system still shows Raman signal if the input polarization is perpendicular to the wire, possibly due to the gap plasmon between the wire and the film. The output polarization dependence showed an interesting and counter-intuitive result that the majority of photons out-coupling from the distal end are polarized not along the wire, but perpendicular to it. This was explored using simulations to gain insight about the underlying physical process. The input power dependence showed Raman signal even for extremely small input power, demonstrating the large field enhancement and nano-focusing that is happening in the cavity between the film and the wire. Finally, numerical simulations were used as a tool to explore the system in ways that were not experimentally feasible, such as

the charge distribution on the wire and the film when excited with various input polarizations. This led to a discovery that when the system is excited with input polarization at  $45^\circ$  to the wire axis, there is generation of chiral plasmons on the film. Thus, simulations were used not only to corroborate the experimental results but also to give new and interesting directions as to what experiments should be done on the system to gain new insights about the system.

This project has, however, not concluded, but opened up a large number of questions that need to be addressed. For example, the system is completely untouched in terms of the Fourier space distribution of the Raman and fluorescence signals that are getting outcoupled at the distal end of the wire. We have done some experiments that suggest that the Raman and fluorescence signals occupy different momentum vectors in the k-space by using Energy-Momentum spectroscopy. However, further experiments are underway to probe this effect in more depth. Theoretical understanding is also required in this case to understand what makes the Raman and fluorescence signals occupy different momentum states in the k-space.

As mentioned in the simulations chapter, the leaky chiral plasmon is another interesting direction in which this project can be taken ahead. The spectroscopic information that we would get from the glass side will be invaluable in itself, and if this can be used to detect chiral dye molecules separately, it would also have an important application. Furthermore, the Fourier space studies of such chiral plasmons have not been done in literature. This is another important question one can ask: how do chiral plasmons look in the k-space?

Single molecule detection and single molecule SERS (SM-SERS) measurement is an extremely important problem, and to be able to detect single molecules with high accuracy and with minimum input power would be a great solution. The system of Ag nanowire-on-gold film shows promise, as the extremely high field enhancement and nano-focusing would allow for such a possibility of SM-SERS.

Apart from all the molecular measurements, the large field enhancements also lead to enhanced metal PL and possibly TPL signals (if one used extremely high input powers). These signals can also be studied in great detail, including polarization dependent studies as well as Fourier space studies, which will show what momentum states are occupied by the PL or the TPL signals, and what directionality is observed for these signals. However, there has been some indication in our experiments that higher input powers lead to what could possibly be signals due to amorphous carbon. These signals are probably due to dissociation of the PVP coating near the wire due to extremely high field intensities. Thus, this problem needs to be taken care of before studying the PL or the TPL in more depth.

To conclude, the project has opened up a large number of new avenues to explore, and these will surely show some very interesting results when followed through.



# References

- [1] A. A. Huurdeman, *The worldwide history of telecommunications*, John Wiley & Sons, 2003.
- [2] G. Marconi, F. Braun, *Nobel lecture: wireless telegraphic communication*, The Nobel Foundation.
- [3] A. A. Maradudin, J. R. Sambles, W. L. Barnes, *Modern plasmonics*, Vol. 4, Elsevier, 2014.
- [4] L. Novotny, N. Van Hulst, *Antennas for light*, *Nature photonics* 5 (2) (2011) 83–90.
- [5] A. G. Curto, G. Volpe, T. H. Taminiau, M. P. Kreuzer, R. Quidant, N. F. van Hulst, *Unidirectional emission of a quantum dot coupled to a nanoantenna*, *Science* 329 (5994) (2010) 930–933.
- [6] T. Kosako, Y. Kadoya, H. F. Hofmann, *Directional control of light by a nano-optical yagi–uda antenna*, *Nature Photonics* 4 (5) (2010) 312–315.
- [7] A. Kinkhabwala, Z. Yu, S. Fan, Y. Avlasevich, K. Müllen, W. Moerner, *Large single-molecule fluorescence enhancements produced by a bowtie nanoantenna*, *Nature Photonics* 3 (11) (2009) 654–657.
- [8] T. R. Jensen, M. D. Malinsky, C. L. Haynes, R. P. Van Duyne, *Nanosphere lithography: tunable localized surface plasmon resonance spectra of silver nanoparticles*, *The Journal of Physical Chemistry B* 104 (45) (2000) 10549–10556.
- [9] J. S. Shumaker-Parry, H. Rochholz, M. Kreiter, *Fabrication of crescent-shaped optical antennas*, *Advanced Materials* 17 (17) (2005) 2131–2134.
- [10] P. Bharadwaj, R. Beams, L. Novotny, *Nanoscale spectroscopy with optical antennas*, *Chemical science* 2 (1) (2011) 136–140.
- [11] R. Gill, L. Tian, W. R. Somerville, E. C. Le Ru, H. van Amerongen, V. Subramaniam, *Silver nanoparticle aggregates as highly efficient plasmonic antennas for fluorescence enhancement*, *The Journal of Physical Chemistry C* 116 (31) (2012) 16687–16693.

- [12] J. Yang, J. You, C.-C. Chen, W.-C. Hsu, H.-r. Tan, X. W. Zhang, Z. Hong, Y. Yang, Plasmonic polymer tandem solar cell, *ACS nano* 5 (8) (2011) 6210–6217.
- [13] M. W. Knight, H. Sobhani, P. Nordlander, N. J. Halas, Photodetection with active optical antennas, *Science* 332 (6030) (2011) 702–704.
- [14] P. Mühlischlegel, H.-J. Eisler, O. Martin, B. Hecht, D. Pohl, Resonant optical antennas, *science* 308 (5728) (2005) 1607–1609.
- [15] D. E. Chang, A. S. Sørensen, P. Hemmer, M. Lukin, Strong coupling of single emitters to surface plasmons, *Physical Review B* 76 (3) (2007) 035420.
- [16] A. G. Curto, T. H. Taminiau, G. Volpe, M. P. Kreuzer, R. Quidant, N. F. Van Hulst, Multipolar radiation of quantum emitters with nanowire optical antennas, *Nature communications* 4 (2013) 1750.
- [17] H. Ditlbacher, A. Hohenau, D. Wagner, U. Kreibig, M. Rogers, F. Hofer, F. R. Aussenegg, J. R. Krenn, Silver nanowires as surface plasmon resonators, *Physical review letters* 95 (25) (2005) 257403.
- [18] J. Dorfmueller, R. Vogelgesang, W. Khunsin, C. Rockstuhl, C. Etrich, K. Kern, Plasmonic nanowire antennas: experiment, simulation, and theory, *Nano letters* 10 (9) (2010) 3596–3603.
- [19] X. Huang, P. K. Jain, I. H. El-Sayed, M. A. El-Sayed, Gold nanoparticles: interesting optical properties and recent applications in cancer diagnostics and therapy, *Nanomedicine* 2 (5) (2007) 681–693.
- [20] Z. Li, F. Hao, Y. Huang, Y. Fang, P. Nordlander, H. Xu, Directional light emission from propagating surface plasmons of silver nanowires, *Nano letters* 9 (12) (2009) 4383–4386.
- [21] T. Ming, L. Zhao, Z. Yang, H. Chen, L. Sun, J. Wang, C. Yan, Strong polarization dependence of plasmon-enhanced fluorescence on single gold nanorods, *Nano letters* 9 (11) (2009) 3896–3903.
- [22] H. Yuan, S. Khatua, P. Zijlstra, M. Yorulmaz, M. Orrit, Thousand-fold enhancement of single-molecule fluorescence near a single gold nanorod, *Angewandte Chemie International Edition* 52 (4) (2013) 1217–1221.
- [23] D. K. Gramotnev, S. I. Bozhevolnyi, Plasmonics beyond the diffraction limit, *Nature photonics* 4 (2) (2010) 83–91.
- [24] S. Mingxia, Surface plasmon propagation in metal nanowires, Ph.D. thesis, Université de Bourgogne (2013).

- [25] W. L. Barnes, A. Dereux, T. W. Ebbesen, Surface plasmon subwavelength optics, *Nature* 424 (6950) (2003) 824–830.
- [26] L. Novotny, B. Hecht, *Principles of nano-optics*, Cambridge university press, 2012.
- [27] S. A. Maier, Localized surface plasmons, *Plasmonics: fundamentals and applications* (2007) 65–88.
- [28] P. Zijlstra, M. Orrit, Single metal nanoparticles: optical detection, spectroscopy and applications, *Reports on Progress in Physics* 74 (10) (2011) 106401.
- [29] M. Hu, C. Novo, A. Funston, H. Wang, H. Staleva, S. Zou, P. Mulvaney, Y. Xia, G. V. Hartland, Dark-field microscopy studies of single metal nanoparticles: understanding the factors that influence the linewidth of the localized surface plasmon resonance, *Journal of materials chemistry* 18 (17) (2008) 1949–1960.
- [30] D. J. Hill, C. W. Pinion, J. D. Christesen, J. F. Cahoon, Waveguide scattering microscopy for dark-field imaging and spectroscopy of photonic nanostructures, *Acs Photonics* 1 (8) (2014) 725–731.
- [31] J. A. Fan, K. Bao, J. B. Lassiter, J. Bao, N. J. Halas, P. Nordlander, F. Capasso, Near-normal incidence dark-field microscopy: applications to nanoplasmonic spectroscopy, *Nano letters* 12 (6) (2012) 2817–2821.
- [32] P. A. Temple, Total internal reflection microscopy: a surface inspection technique, *Applied Optics* 20 (15) (1981) 2656–2664.
- [33] J. W. Ha, K. Marchuk, N. Fang, Focused orientation and position imaging (fopi) of single anisotropic plasmonic nanoparticles by total internal reflection scattering microscopy, *Nano letters* 12 (8) (2012) 4282–4288.
- [34] K. A. Koen, M. L. Weber, K. M. Mayer, E. Fernandez, K. A. Willets, Spectrally-resolved polarization anisotropy of single plasmonic nanoparticles excited by total internal reflection, *The Journal of Physical Chemistry C* 116 (30) (2012) 16198–16206.
- [35] C. Sönnichsen, S. Geier, N. Hecker, G. Von Plessen, J. Feldmann, H. Ditlbacher, B. Lamprecht, J. Krenn, F. Aussenegg, V. Z. Chan, et al., Spectroscopy of single metallic nanoparticles using total internal reflection microscopy, *Applied Physics Letters* 77 (19) (2000) 2949–2951.
- [36] J. J. Mock, R. T. Hill, Y.-J. Tsai, A. Chilkoti, D. R. Smith, Probing dynamically tunable localized surface plasmon resonances of film-coupled nanoparticles by evanescent wave excitation, *Nano letters* 12 (4) (2012) 1757–1764.

- [37] J. Zhang, J. Malicka, I. Gryczynski, J. R. Lakowicz, Surface-enhanced fluorescence of fluorescein-labeled oligonucleotides capped on silver nanoparticles, *The Journal of Physical Chemistry B* 109 (16) (2005) 7643–7648.
- [38] A. R. Guerrero, R. F. Aroca, Surface-enhanced fluorescence with shell-isolated nanoparticles (shinef), *Angewandte Chemie International Edition* 50 (3) (2011) 665–668.
- [39] A. Campion, P. Kambhampati, Surface-enhanced raman scattering, *Chemical Society Reviews* 27 (4) (1998) 241–250.
- [40] P. L. Stiles, J. A. Dieringer, N. C. Shah, R. P. Van Duyne, Surface-enhanced raman spectroscopy, *Annu. Rev. Anal. Chem.* 1 (2008) 601–626.
- [41] H. Wei, F. Hao, Y. Huang, W. Wang, P. Nordlander, H. Xu, Polarization dependence of surface-enhanced raman scattering in gold nanoparticle- nanowire systems, *Nano letters* 8 (8) (2008) 2497–2502.
- [42] A. V. Zayats, I. I. Smolyaninov, A. A. Maradudin, Nano-optics of surface plasmon polaritons, *Physics reports* 408 (3) (2005) 131–314.
- [43] A. V. Zayats, I. I. Smolyaninov, Near-field photonics: surface plasmon polaritons and localized surface plasmons, *Journal of Optics A: Pure and Applied Optics* 5 (4) (2003) S16.
- [44] Y. Fang, H. Wei, F. Hao, P. Nordlander, H. Xu, Remote-excitation surface-enhanced raman scattering using propagating ag nanowire plasmons, *Nano letters* 9 (5) (2009) 2049–2053.
- [45] Y. Sun, B. Gates, B. Mayers, Y. Xia, Crystalline silver nanowires by soft solution processing, *Nano letters* 2 (2) (2002) 165–168.
- [46] Y. Sun, Y. Yin, B. T. Mayers, T. Herricks, Y. Xia, Uniform silver nanowires synthesis by reducing agno<sub>3</sub> with ethylene glycol in the presence of seeds and poly (vinyl pyrrolidone), *Chemistry of Materials* 14 (11) (2002) 4736–4745.
- [47] A. W. Sanders, D. A. Routenberg, B. J. Wiley, Y. Xia, E. R. Dufresne, M. A. Reed, Observation of plasmon propagation, redirection, and fan-out in silver nanowires, *Nano letters* 6 (8) (2006) 1822–1826.
- [48] M. Song, A. Bouhelier, P. Bramant, J. Sharma, E. Dujardin, D. Zhang, G. Colas-des Francs, Imaging symmetry-selected corner plasmon modes in penta-twinned crystalline ag nanowires, *ACS nano* 5 (7) (2011) 5874–5880.
- [49] D. K. Gramotnev, S. I. Bozhevolnyi, Nanofocusing of electromagnetic radiation, *Nature Photonics* 8 (1) (2014) 13–22.

- [50] C. L. Smith, N. Stenger, A. Kristensen, N. A. Mortensen, S. I. Bozhevolnyi, Gap and channeled plasmons in tapered grooves: a review, *Nanoscale* 7 (21) (2015) 9355–9386.
- [51] A. Bek, R. Jansen, M. Ringler, S. Mayilo, T. A. Klar, J. Feldmann, Fluorescence enhancement in hot spots of afm-designed gold nanoparticle sandwiches, *Nano Letters* 8 (2) (2008) 485–490.
- [52] G. M. Akselrod, C. Argyropoulos, T. B. Hoang, C. Ciraci, C. Fang, J. Huang, D. R. Smith, M. H. Mikkelsen, Probing the mechanisms of large purcell enhancement in plasmonic nanoantennas, *Nature Photonics* 8 (11) (2014) 835–840.
- [53] K. J. Vahala, Optical microcavities, *Nature* 424 (6950) (2003) 839–846.
- [54] Theory of raman scattering, <http://bwtek.com/raman-theory-of-raman-scattering/>.
- [55] K. Kneipp, H. Kneipp, H. G. Bohr, Single-molecule sers spectroscopy, in: *Surface-Enhanced Raman Scattering*, Springer, 2006, pp. 261–277.
- [56] K. Kneipp, Y. Wang, H. Kneipp, L. T. Perelman, I. Itzkan, R. R. Dasari, M. S. Feld, Single molecule detection using surface-enhanced raman scattering (sers), *Physical review letters* 78 (9) (1997) 1667.
- [57] G. von Maltzahn, A. Centrone, J.-H. Park, R. Ramanathan, M. J. Sailor, T. A. Hatton, S. N. Bhatia, Sers-coded gold nanorods as a multifunctional platform for densely multiplexed near-infrared imaging and photothermal heating, *Advanced Materials* 21 (31) (2009) 3175–3180.
- [58] E. Le Ru, P. Etchegoin, Rigorous justification of the  $\times 4$  enhancement factor in surface enhanced raman spectroscopy, *chemical Physics letters* 423 (1) (2006) 63–66.
- [59] K. J. Russell, T.-L. Liu, S. Cui, E. L. Hu, Large spontaneous emission enhancement in plasmonic nanocavities, *Nature Photonics* 6 (7) (2012) 459–462.
- [60] N. Félidj, J. Grand, G. Laurent, J. Aubard, G. Levi, A. Hohenau, N. Galler, F. Aussenegg, J. Krenn, Multipolar surface plasmon peaks on gold nanotriangles, *The Journal of chemical physics* 128 (9) (2008) 094702.
- [61] J. E. Millstone, S. Park, K. L. Shuford, L. Qin, G. C. Schatz, C. A. Mirkin, Observation of a quadrupole plasmon mode for a colloidal solution of gold nanoprisms, *Journal of the American Chemical Society* 127 (15) (2005) 5312–5313.
- [62] Z. Li, Y. Yu, Z. Chen, T. Liu, Z.-K. Zhou, J.-B. Han, J. Li, C. Jin, X. Wang, Ultrafast third-order optical nonlinearity in au triangular nanoprism with strong dipole and quadrupole plasmon resonance, *The Journal of Physical Chemistry C* 117 (39) (2013) 20127–20132.

- [63] A. Tcherniak, S. Dominguez-Medina, W.-S. Chang, P. Swanglap, L. S. Slaughter, C. F. Landes, S. Link, One-photon plasmon luminescence and its application to correlation spectroscopy as a probe for rotational and translational dynamics of gold nanorods, *The Journal of Physical Chemistry C* 115 (32) (2011) 15938–15949.
- [64] A. Bouhelier, R. Bachelot, G. Lerondel, S. Kostcheev, P. Royer, G. Wiederrecht, Surface plasmon characteristics of tunable photoluminescence in single gold nanorods, *Physical review letters* 95 (26) (2005) 267405.
- [65] K. Imura, T. Nagahara, H. Okamoto, Plasmon mode imaging of single gold nanorods, *Journal of the American Chemical Society* 126 (40) (2004) 12730–12731.
- [66] K. Imura, T. Nagahara, H. Okamoto, Near-field two-photon-induced photoluminescence from single gold nanorods and imaging of plasmon modes, *The Journal of Physical Chemistry B* 109 (27) (2005) 13214–13220.
- [67] D.-S. Wang, F.-Y. Hsu, C.-W. Lin, Surface plasmon effects on two photon luminescence of gold nanorods, *Optics express* 17 (14) (2009) 11350–11359.
- [68] C. Hubert, L. Billot, P.-M. Adam, R. Bachelot, P. Royer, J. Grand, D. Gindre, K. Dorkenoo, A. Fort, Role of surface plasmon in second harmonic generation from gold nanorods, *Applied physics letters* 90 (18) (2007) 181105.
- [69] W. Rechberger, A. Hohenau, A. Leitner, J. Krenn, B. Lamprecht, F. Aussenegg, Optical properties of two interacting gold nanoparticles, *Optics communications* 220 (1) (2003) 137–141.
- [70] J. Kimling, M. Maier, B. Okenve, V. Kotaidis, H. Ballot, A. Plech, Turkevich method for gold nanoparticle synthesis revisited, *The Journal of Physical Chemistry B* 110 (32) (2006) 15700–15707.
- [71] L. Chen, F. Ji, Y. Xu, L. He, Y. Mi, F. Bao, B. Sun, X. Zhang, Q. Zhang, High-yield seedless synthesis of triangular gold nanoplates through oxidative etching, *Nano letters* 14 (12) (2014) 7201–7206.
- [72] A. Gole, C. J. Murphy, Seed-mediated synthesis of gold nanorods: role of the size and nature of the seed, *Chemistry of Materials* 16 (19) (2004) 3633–3640.
- [73] J. J. Mock, R. T. Hill, A. Degiron, S. Zauscher, A. Chilkoti, D. R. Smith, Distance-dependent plasmon resonant coupling between a gold nanoparticle and gold film, *Nano letters* 8 (8) (2008) 2245–2252.
- [74] P. G. Etchegoin, E. C. Le Ru, Resolving single molecules in surface-enhanced raman scattering within the inhomogeneous broadening of raman peaks, *Analytical chemistry* 82 (7) (2010) 2888–2892.

- [75] S. Narayanan, G. Cheng, Z. Zeng, Y. Zhu, T. Zhu, Strain hardening and size effect in five-fold twinned ag nanowires, *Nano letters* 15 (6) (2015) 4037–4044.
- [76] B. Wiley, Y. Sun, B. Mayers, Y. Xia, Shape-controlled synthesis of metal nanostructures: the case of silver, *Chemistry–A European Journal* 11 (2) (2005) 454–463.
- [77] J. Hwang, Y. Shim, S.-M. Yoon, S. H. Lee, S.-H. Park, Influence of polyvinylpyrrolidone (pvp) capping layer on silver nanowire networks: theoretical and experimental studies, *RSC Advances* 6 (37) (2016) 30972–30977.
- [78] H. Gommans, J. Alldredge, H. Tashiro, J. Park, J. Magnuson, A. Rinzler, Fibers of aligned single-walled carbon nanotubes: Polarized raman spectroscopy, *Journal of Applied Physics* 88 (5) (2000) 2509–2514.
- [79] R. Chikkaraddy, D. Singh, G. Pavan Kumar, Plasmon assisted light propagation and raman scattering hot-spot in end-to-end coupled silver nanowire pairs, *Applied Physics Letters* 100 (4) (2012) 043108.
- [80] A. Dasgupta, D. Singh, S. Tandon, R. P. Tripathi, G. P. Kumar, Remote-excitation surface-enhanced raman scattering with counter-propagating plasmons: silver nanowire-nanoparticle system, *Journal of Nanophotonics* 8 (1) (2014) 083899–083899.
- [81] T. Shegai, V. D. Miljkovic, K. Bao, H. Xu, P. Nordlander, P. Johansson, M. Kall, Unidirectional broadband light emission from supported plasmonic nanowires, *Nano letters* 11 (2) (2011) 706–711.
- [82] E. Le Ru, P. Etchegoin, *Principles of Surface-Enhanced Raman Spectroscopy: and related plasmonic effects*, Elsevier, 2008.
- [83] Z. Li, K. Bao, Y. Fang, Y. Huang, P. Nordlander, H. Xu, Correlation between incident and emission polarization in nanowire surface plasmon waveguides, *Nano letters* 10 (5) (2010) 1831–1835.
- [84] D. Logan, *First course in finite element analysis*, Brooks/Cole.
- [85] P. B. Johnson, R.-W. Christy, Optical constants of the noble metals, *Physical review B* 6 (12) (1972) 4370.
- [86] M. Sun, Z. Zhang, P. Wang, Q. Li, F. Ma, H. Xu, Remotely excited raman optical activity using chiral plasmon propagation in ag nanowires, *Light: Science & Applications* 2 (11) (2013) e112.
- [87] B. Wang, J. Zhou, T. Koschny, M. Kafesaki, C. M. Soukoulis, Chiral metamaterials: simulations and experiments, *Journal of Optics A: Pure and Applied Optics* 11 (11) (2009) 114003.

- [88] M. Schäferling, D. Dregely, M. Hentschel, H. Giessen, Tailoring enhanced optical chirality: design principles for chiral plasmonic nanostructures, *Physical Review X* 2 (3) (2012) 031010.
- [89] Z. Fan, A. O. Govorov, Plasmonic circular dichroism of chiral metal nanoparticle assemblies, *Nano letters* 10 (7) (2010) 2580–2587.